a Coriolis tutorial, Part 5:

on the seasonally-varying circulation of the Arabian Sea

James F. Price

Woods Hole Oceanographic Institution,
Woods Hole, Massachusetts, 02543
https://www2.whoi.edu/staff/jprice/ jprice@whoi.edu

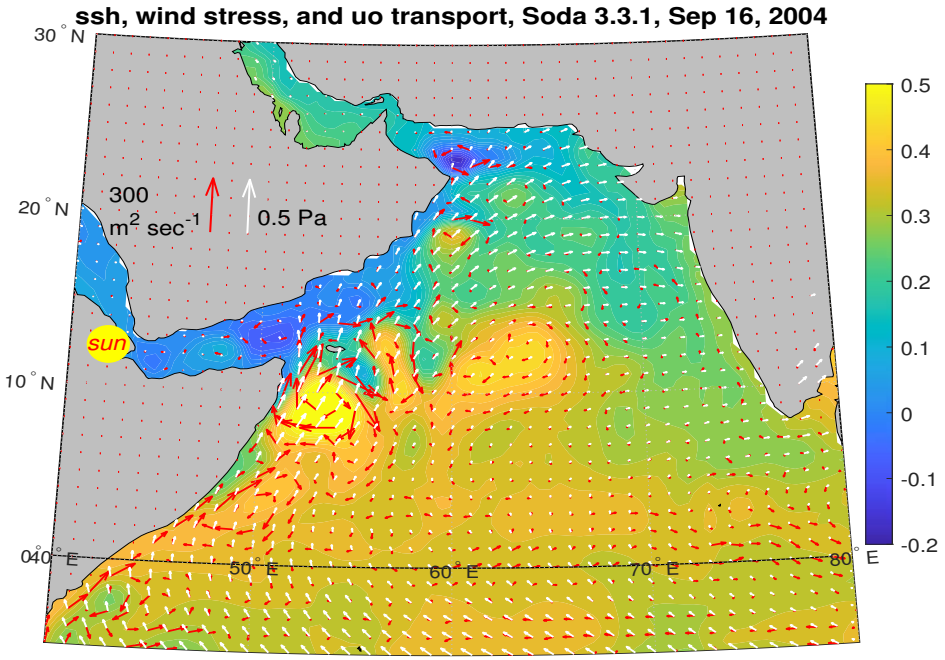

Figure 1: A snapshot from an animation of winds and ocean circulation of the Arabian Sea https://www2.whoi.edu/staff/jprice/AS-winds/ These data are from the Soda 3.3.1 reanalysis discussed below. The background is Soda-computed sea surface height, with a color bar at right in meters. The white vector field is wind stress from satellite scatterometry, with a scale vector at left. The red vectors are upper ocean transport, with a scale at left. The animation runs from January 2004 to January 2005. This frame is from mid-September 2004 and shows a typical summer circulation — a high over the central and western Arabian Sea, that is significantly perturbed by large eddies. The yellow disk that slides up and down the left side of the frame indicates the sun's declination. This figure and the accompanying animation will probably be overwhelming on first sight. An implicit goal of this essay is that you be able to interpret and anticipate much of what you see here.

Contents

1 Seasonal variability of the Arabian Sea

The North Indian Ocean (NIO) is the only major ocean that did not appear in the list of basin-scale, time-mean gyres compiled as Table 1 of Part 4, since its annual mean circulation is not representative of an observable state. The NIO offers something different, and for our purpose, something better — a *seasonally-varying* circulation that is mainly a response to seasonally-reversing winds. Winter and summer circulation patterns are qualitatively different (Fig. 2) and largely repeatable from year to year. The summer circulation is especially interesting as it is the outstanding example of a significant, wind-driven circulation that is generated anew each year.

The object here is to offer a concise description of some of the remarkable phenomena that make up the Arabian Sea circulation, Fig. (3), both winter and summer. The specific goal is to explain as simply as possible (but not simpler) the link between the wind and the vigorous, summertime circulation.[1]

1.1 The plan/summary

1.1.1 A description of the winds and the ocean circulation phenomena of the Arabian Sea

The data sources that make this study possible are reviewed briefly in Sec. 2, and the all-important South Asia Monsoon winds are introduced in Sec. 3. The monsoon winds are different in almost every respect from the midlatitude winds of the North Atlantic; there is modest northeast wind over most of the Arabian Sea during the winter, and then very strong southwest winds develop during the summer. This seasonality has a profound effect upon the physical oceanography of the Arabian Sea, which is introduced in Sec. 4. The summertime circulation includes a compact anticyclonic gyre in the interior of the basin, and a poleward western boundary current, the Somali Current, which has meridional transport of about 30 Sv. There are several large anticyclonic eddies that recur in most summers, including the very strong Great Whirl. The wintertime circulation has by comparison a modest amplitude, meridional transport of roughly 10 Sv, and shows a significant influence of remote forcing coming from the Bay of Bengal.

[1] An excellent entree to descriptive oceanography of this region is the text by Talley, L., G. Pickard, W. Emery and J. Swift, 2011, Descriptive Physical Oceanography, Elsevier, ISBN:9780750645522. Some of the pioneering estimates of circulation amplitude and time-dependence are reported by Düing, W. and H. Szekielda (1970) Monsoonal response in the western Indian Ocean, J. Geophys. Res., 76, 4181-4187. An insightful and accessible research paper that anticipates much of what is found here is by Bruce, J. G., 1983, The wind field in the western Indian Ocean and the related ocean circulation. Mon. Wea. Rev., 111, 1442 - 1452. Also very useful is Shetye, S.R., Gouveia, A.D. and Shenoi, S.S.C., 1994, Circulation and water masses of the Arabian Sea. Proc. Indian Acad. Sci. (Earth Planet Sci.) 103, 107 - 123. https://doi.org/10.1007/BF02839532. A comprehensive and authoritative research review of the entire Indian Ocean is by Schott, F. A. and J. P. McCreary Jr., 2001, The monsoon circulation of the Indian Ocean, Prog. in Oceanogr., 51, 1 - 123.

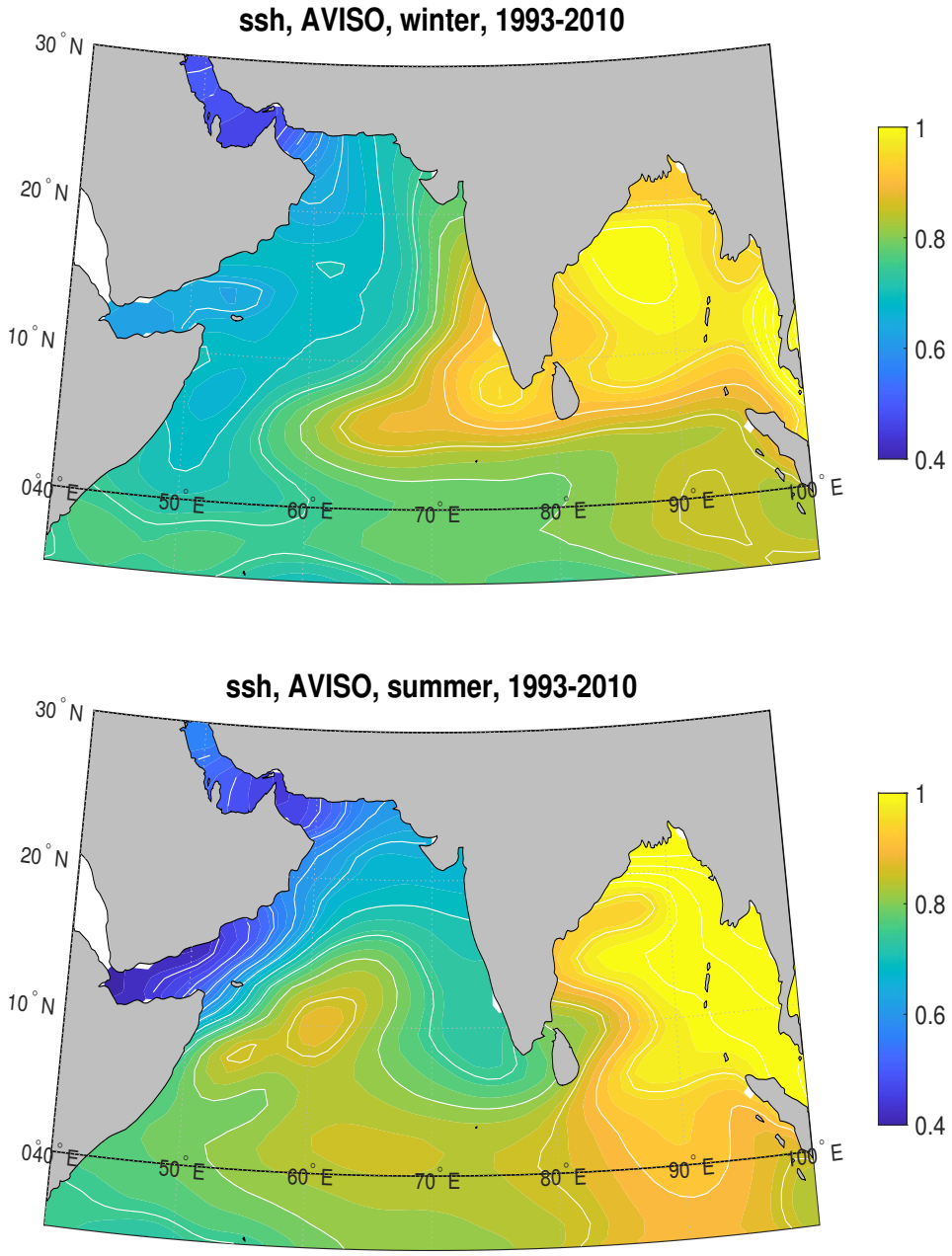

Figure 2: Seasonal averages of sea surface height observed by satellite altimetry and analyzed and archived by the AVISO project (https://www.aviso.altimetry.fr). These data are from the already smoothed (one degree, monthly) AVISO Level 4 analysis that was then composite averaged over winters **(upper)** and summers **(lower)** of almost two decades, 1993-2010. The colorbar at right is in meters. In the winter, high ssh emanates from the Bay of Bengal and spreads northward along the west coast of India and westward across the Arabian Sea along about 6 N latitude. The resulting 6 N ridge is said to be the result of remote forcing from the Bay of Bengal. In the summer, there is a compact high of ssh in the central basin of the Arabian Sea, centered on 10 N, 62 E. This summertime ssh high and the associated circulation are consistent with local and basinwide wind forcing.

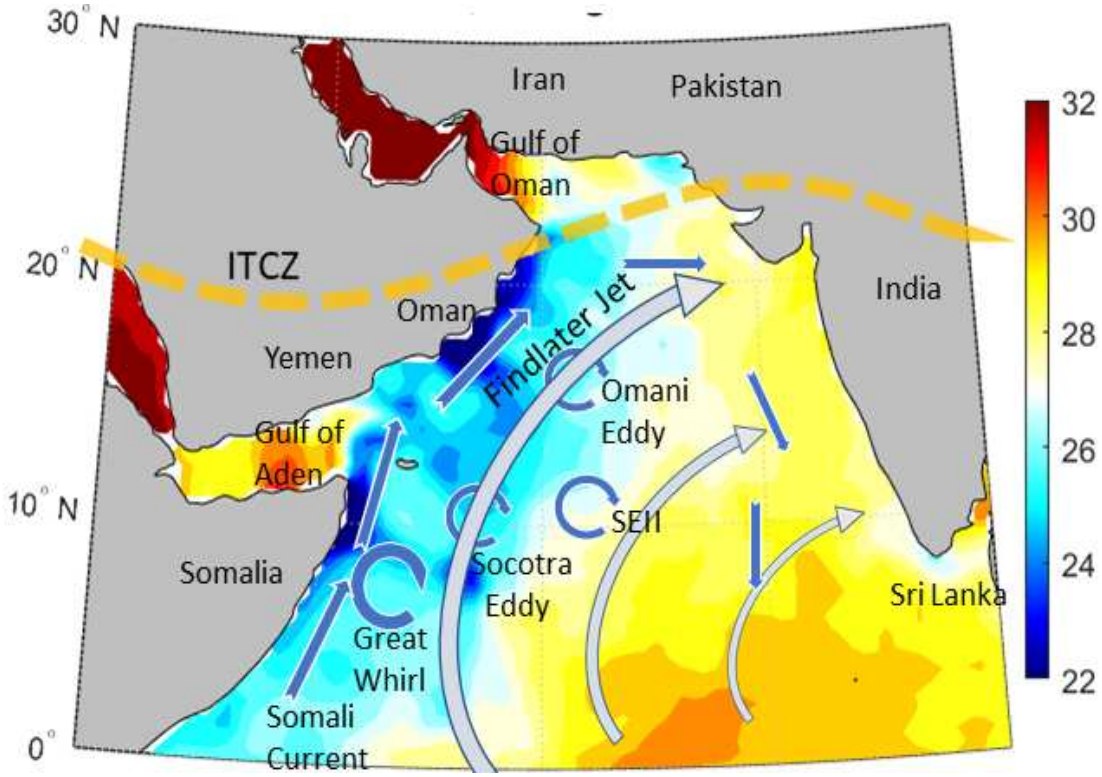

Figure 3: A schematic of the Arabian Sea during the summer, showing a number of the features discussed here. The background is the actual observed SST from mid August, 2021, with a color scale in degrees C at right. Meteorology includes the low pressure trough of the Intertropical Convergence Zone (ITCZ, heavy yellow dashed line), which in summer is near the northern edge of the Arabian Sea, and the Findlater Jet (the clockwise turning gray vector), which is a significant local maximum of the Southwest Monsoon winds. Notable oceanographic features include very cool SST in the coastal upwelling regions offshore of Somalia and Oman, a northward flowing western boundary current called the Somali Current, a large and intense anticyclone offshore of Somalia called the Great Whirl, and a somewhat weaker but still significant anticyclone called the Socotra Eddy. Two other anticyclones that appear in many years are also noted, SEII, a neighbor of the Socotra Eddy, and the Omani Eddy to the north. During boreal winter, the ITCZ is displaced well to the south of the equator, and the winds over the Arabian Sea are then reversed and weakened considerably compared to the summer winds depicted here — these oceanographic features soon disappear.

1.1.2 Explaining the link between the wind and the summer circulation

The scope then narrows to address where, when and why there is meridional flow into the Arabian Sea across 10 N latitude. Despite the complication of eddies and remote forcing, the Sverdrup relation is found to give a good account of the meridional transport during the summer, when the winds and the transport are largest, but not during the winter, Sec. 5. Even a partial success is somewhat surprising — why is the time-independent Sverdrup relation relevant to this seasonally-varying circulation? The explanation offered here comes in two steps. First is the recognition that the circulation, measured by the western boundary current, responds very quickly to the onset of Southwest Monsoon winds,[1] within only a few weeks, Sec. 5.3, and thus the circulation is not far from steady state with respect to a seasonally-varying wind. This rapid response of the Arabian Sea may be compared to the western boundary current of a typical mid-latitude basin, which requires about five years to reach nearly full speed (estimated from the baroclinic model results of Sec. 5.3, Part 4). The ratio of response times of the Arabian Sea vs. a mid-latitude gyre is thus about two orders of magnitude. The second step is to offer a simple (as possible, but not too simple) explanation of this very large difference. Useful guidance comes from start-up experiments that include a jet-like windfield, Sec. 6. The most important factor appears to be the low latitude of the Arabian Sea and the $1/f^2$ dependence of locally-wind forced geostrophic currents (Sec. 5.2, Part 4).[2] A second important factor comes from the western-biased and jet-like form of the Southwest Monsoon wind field, which imposes a zonal length scale that is much less than the width of the basin. The fast response of the model Arabian Sea is consistent with small amplitude (linear) dynamics. Finite amplitude (nonlinear) effects appear to be very important in the formation of an intense, mesoscale anticyclone that has some properties in common with the Great Whirl discused briefly in Sec. 7. The final section, 8, points out several of the more important limitations of this study.

1.2 About this essay

The tenor of this discussion is academic and pedagogic insofar as the aim is enhanced understanding for its own sake. Like Parts 1 - 4, it has been written for students who are beginning a study of geophysical fluid dynamics. It is meant to be somewhat self-contained, but draws upon many of the concepts and results of Parts 3 and 4.

The topic is one of great societal interest. The climate and the weather of the South Asia monsoon affect the lives of everyone living around the Indian Ocean, roughly a third of the world's population.

[2]This very important latitudinal dependence was discussed by Lighthill, M. J. (1969) Dynamic response of the Indian Ocean to onset of the southwest monsoon, Phil Trans. Roy. Soc. of London, Vol. 265, No. 1159, 45-92. Lighthill's paper is a landmark, written before the advent of remote sensing and the widespread use of numerical modelling; do not be discouraged if you find it a difficult read. An early, interesting numerical modelling study of the monsoon response was by Hurlbert, H. E., and J. D. Thompson (1976) A numerical model of the Somali Current, J. Phys. Oceanogr., 6, 646-664. A very wide-ranging and thorough modeling study is by McCreary, J. P., P. K. Kundu and R. L. Molinari (1993) A numerical investigation of dynamics, thermodynamics and mixed-layer processes in the Indian Ocean, Prog. Oceanog., 31, 181-224. More recent is an in-depth study by Wang, H., J. L. McClean, L. D. Talley and S. Yeager (2018) Seasonal cycle and annual reversal of the Somali Current in an eddy-resolving global ocean model, J. Geophys. Res-Oceans, 123, 6562-6580.

The timing and the amplitude of the Southwest Monsoon onset is especially important; alongshore, upwelling favorable winds induce an ocean bloom along the coasts of Somalia and Oman that supports a major fishery (the very cool SST along the western boundary of Fig. 3). The flow of relatively moist maritime air onto the Indian subcontinent ends a wintertime drought, and is the vital source of fresh water to the subcontinent. Improved understanding of the ocean and atmosphere that could lead to better forecasting of these phenomena is the prime motive for ongoing, innovative research in this region.[3]

Acknowledgments. Financial support during the preparation of these essays was provided by the Academic Programs Office of the Woods Hole Oceanographic Institution. Additional salary support has been provided by the U.S. Office of Naval Research. My thanks to Kenneth Brink, Viviane Menezes, Robert Todd and Alex Kinsella of the Woods Hole Oceanographic Institution and to Amit Tandon of University of Massachusetts at Dartmouth for their valuable comments on a draft of this essay. Administrative support was provided by Woods Hole Oceanographic Administration.

Author's note. You may notice that this essay differs from the previous four parts of a Corolis tutorial in that it reads more like a research report than an introductory-level textbook; there is a greater emphasis on attribution than is necessary in a textbook, and you may detect a sense of discovery. This stems mainly from the topic being a new one for me; I was learning along the way, as I hope you will too.

This study is dedicated to Dr. Walter O. Düing, RSMAS, University of Miami, whose enthusiasm for observational oceanography and for the Arabian Sea has been a lasting inspiration.

2 Data sources: SODA and AVISO

This description of Arabian Sea winds and currents is built with three kinds of data from three sources.

[3]Centurioni, L.R. et al. (2017) Northern Arabian Sea Circulation-Autonomous Research (NASCar): A research initiative based on autonomous sensors. Oceanography 30(2):7487, https://doi.org/?10.5670/oceanog.2017.224, and Todd, R. E. (2020). Equatorial circulation in the western Indian Ocean during onset of the 2018 summer monsoon and links to the Bay of Bengal. Geophysical Research Letters, 47, e2020GL087215. https://doi.org/10.1029/2020GL087215. The surface layer response to wind-forcing and the resulting impacts upon bio-relevant properties are examined by Lee, C. M., B. H. Jones, K. H. Brink and A. S. Fischer (2000), The upper-ocean response to monsoonal forcing in the Arabian Sea: seasonal and spatial variability, Deep Sea Res, Part II, 47(7), 1177-1226. An up to date and comprehensive presentation of ongoing research is by Phillips, H. E. and colleagues (2021), Progress in understanding Indian Ocean circulation, variability, air-sea exchange and impacts on biogeochemistry, Ocean Science Discussions, EGU, https://doi.org/10.5194/os-2021-1.

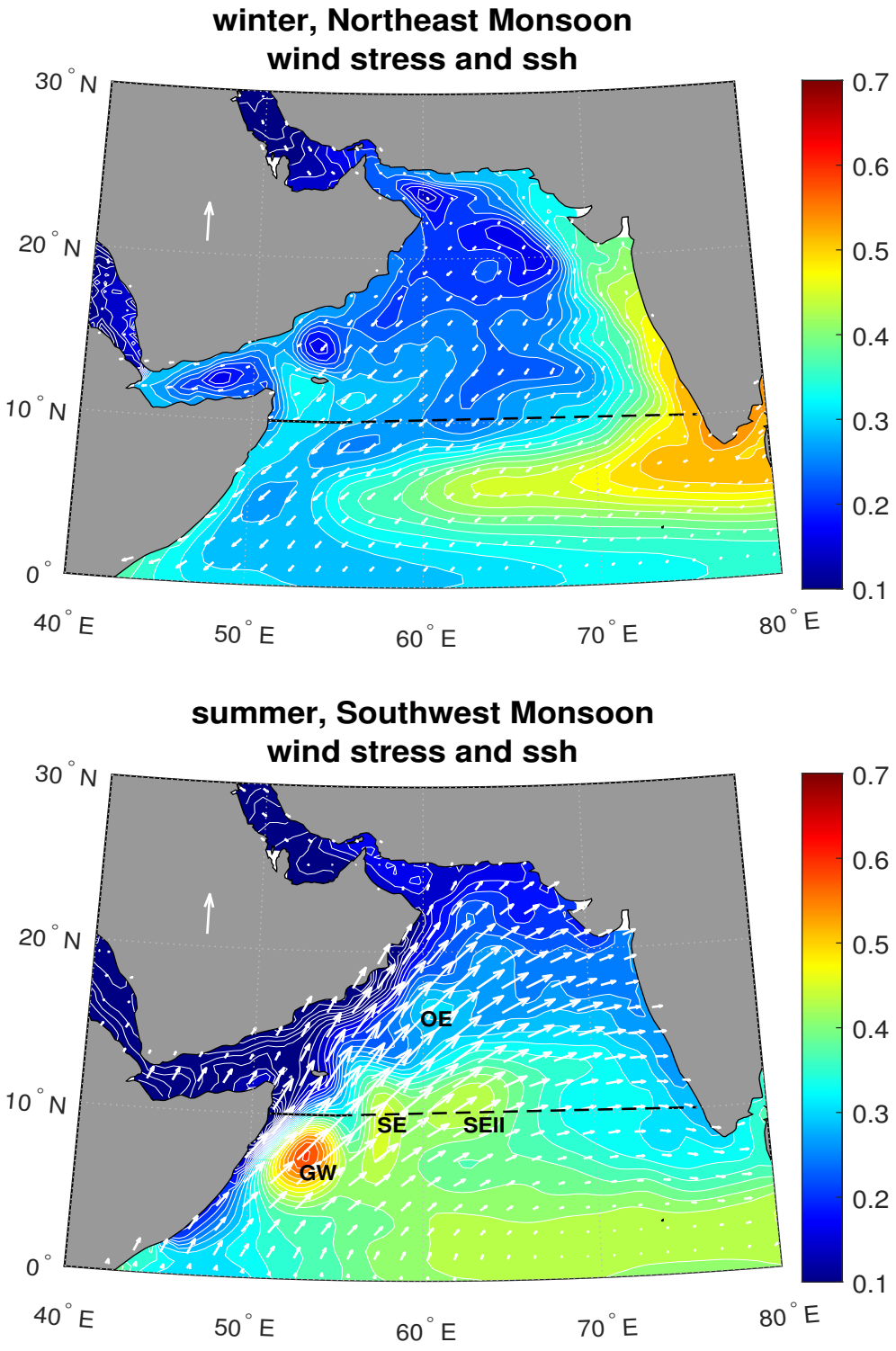

Figure 4: Winter **(upper)** and summer **(lower)** over the Arabian Sea. The white vectors are wind stress from scatterometry reported by SODA 3.3.1; the isolated vector over the Arabian peninsula has an amplitude of 0.3 Pa. The colored background is ssh computed by the SODA 3.3.1 surface reanalysis. The colorbar at right is in meters. The seasons were composite-averaged over two decades starting in 1990. The black solid and dashed line along 10 N is the open boundary of an Arabian Sea control volume defined in Sec. 4. In the upper panel, notice the ridge of high ssh (yellow and orange) that extends westward from the southern tip of India during winter, and in the lower panel, the intense, almost circular high (red bullseye) at about the same latitude during the summer, the Great Whirl, GW. Three other eddies are also noted in summer, SE, SEII and OE, and discussed below.

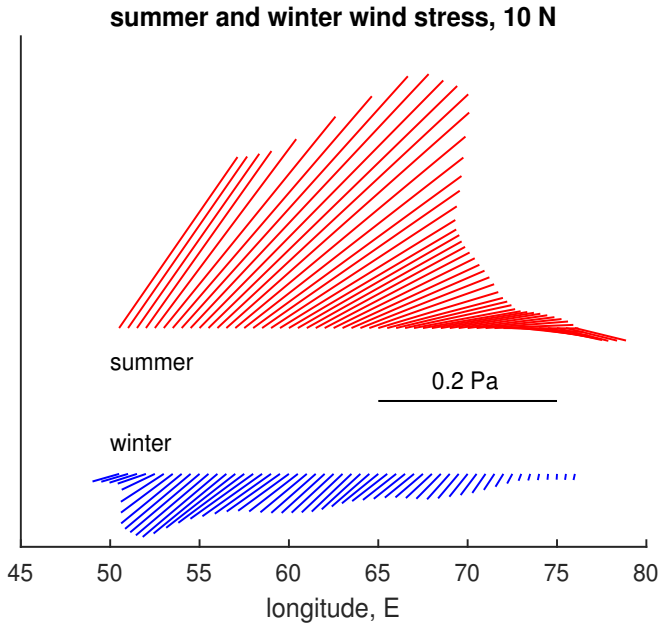

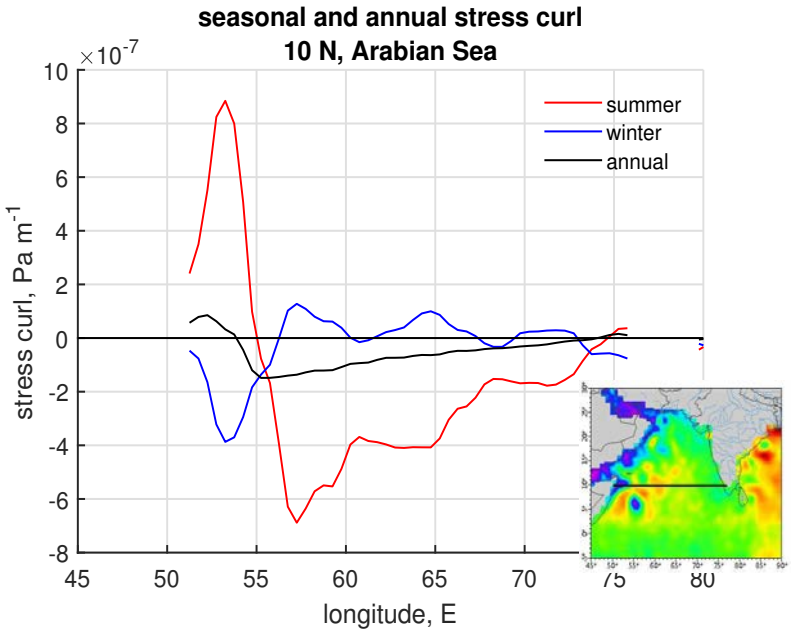

Figure 5: **(upper)** Wind stress along 10 N from the SODA 3.3.1 reanalysis of sea surface properties. North is up, and the magnitude may be compared to the black line segment labeled 0.2 Pa. The maximum of wind stress is at about 55 E in both summer and winter; the summer maximum is known as the Findlater Jet. **(lower)** Wind stress curl along 10 N by seasons and on annual average. Wind stress curl changes sign across the jet axis.

- **Wind stress from satellite scatterometery**, as reported by the SODA 3.3.1 surface reanalysis[4].[4] Wind stress is regarded as external and given. These are the data of Fig. (4).

- **Sea surface height from satellite altimetry** that has been analyzed and archived by the AVISO project, especially the smoothed and averaged (one degree, monthly) Level 4 analysis (Fig. 2) prepared for climate model intercomparisons.[5] This data set is a synthesis of the measurements made by five altimetric satellites and referenced to a geoid. It is highly reliable, however the smoothing does suppress some smaller scale, O(200 km), variability that shows up well in other, less smoothed data sets.

- **Ocean currents and sea surface height computed by the SODA 2.2.4 reanalysis.** These data are the solution of a comprehensive Ocean GCM that was continually updated and made to be consistent with a wide range of oceanic and atmospheric observations including scatterometry-derived wind stress, satellite-derived SST, and many types of *in situ* temperature and salinity observations, but not ocean currents or ssh.[6] The SODA data are served at 1/2 degree intervals in latitude and longitude and at depths from very near the surface where the sampling interval is 10 m, all the way down to the sea floor at almost 5 km depth where the depth interval is a few hundred meters. Monthly-averaged velocity is available from the two decade period beginning 1990. The huge appeal of these reanalysis data (compared with actual, obtainable ocean field observations) is that they are fully four-dimensional, e.g., the meridional velocity component v is $v(x,y,z,t)$ at tens of millions of discrete points and over almost the entire ocean. From the SODA data archive it is possible to estimate of volume transport, heat transport, etc., that are generally not resolved well by ocean observations standing alone. To describe *where* and *when* there is ocean circulation we need only make an intelligible presentation of these invaluable data; to explain *why* there is ocean circulation, we will work toward an understanding of the link between currents and the wind. This will involve models.

2.1 SODA ssh compared with AVISO observed ssh

It is outside the scope here to attempt a thorough ground-truthing of SODA data (see Carton et al., 1988[4]), but a consistency check is highly desirable, and can be made against AVISO observed sea surface height since it was not incorporated within the reanalysis process. A comparison of the SODA-computed ssh (Fig. 4) with the AVISO-analyzed, smoothed ssh (Fig. 2) suggests that large scale features (several hundreds of kilometers or greater) are in common between these two independent realizations. This is a

[4]Carton, J. A., G. A. Chepurin and L. Chen, 2018. SODA3: A new ocean climate reanalysis. *J. Clim.*, Vol. 31, 6967-6983.

[5]Details and the data itself are at https://doi.org/10.5067/DYNTO-1D1M1

[6]The reason for omitting satellite altimeter-derived ssh is interesting and relevant. Even a rather small error in ssh that is imposed upon an OGCM will cause large errors in deep ocean currents and thus in the total transport. However, if the altimetric data are averaged long enough in space and time to suppress random noise, then it will likely be at the expense of genuine mesoscale variability. There are presently two versions of AVISO ssh that are served on the ERDDAP web page and that illustrate this tradeoff between resolution and reliability; a high resolution version (quarter degree spatial resolution and 5 day temporal sampling) and a lower resolution version (one degree spatial and monthly temporal) that was used to make Fig. (2).

positive consistency check on the SODA ssh and the SODA reanalysis generally. There are some significant smaller scale features that are suppressed in the smoothed AVISO L4 analysis, but more on this below.

2.2 Transport and volume transport

Ocean circulation will be represented mainly by the transport, **M**, [m^2 sec^{-1}], a two component vector field,

$$ {}^{x}M(x,\ y,\ t) \ = \ \int_{-b}^{0} u(x,y,z,t)\ dz, \qquad \text{and} \qquad {}^{y}M(x,\ y,\ t) \ = \ \int_{-b}^{0} v(x,y,z,t)\ dz. $$

(A more descriptive but tedious name for this is volume transport per unit width.) If, as here, the vertical integral is over the full water column, then this will be called the total transport, or sometimes just transport. Alternatively, if the vertical integral is over the shallowest 400 m only,

$$ {}^{y}_{uo}M(x,\ y,\ t) \ = \ \int_{-400}^{0} v(x,y,z,t)\ dz, $$

then the result is said to be the upper ocean transport.

The three-dimensional $\mathbf{M}(x,y,t)$ can be displayed via an animation.[7] More often, the transport will be time averaged or space averaged in one of several ways; a simple time average over the full record length, 1990 - 2010, T,

$$ {}^{y}M(x,\ y)^{ann} \ = \ \frac{1}{T}\int_{1990}^{2010} {}^{y}M(x,\ y,\ t)\ dt, $$

and called the annual average, or a composite average over a given season, all of the winters (November, December and January) of 1990 - 2010, ${}^{y}M(x,y)^{win}$, or all of the summers (June, July, August), ${}^{y}M(x,y)^{sum}$, Fig. (6), upper and lower. On each instance of integrating (or averaging) there is a gain in simplicity made by eliminating unwanted and inessential details. Of course, what is inessential may not be obvious, and will certainly depend upon the context.

Two kinds of current profiles. The distinction between total transport and upper ocean transport can be a valuable diagnostic that will be used here on several occasions.

- **Equivalent barotropic:** In the case of a steady, wind-driven Sverdrup flow, the total transport is mainly within the upper ocean. Deeper flow, while it may be very weak, is in the same direction (Sec. 8.4, Part 4, and the Sverdrup flow of the North Atlantic subtropical gyre). The current profile is thus unidirectional and surface-intensified, sometimes referred to as 'equivalent barotropic' flow. In that event, the total transport and the upper ocean transport will be similar in magnitude and direction.

[7] https://www2.whoi.edu/staff/jprice/as-transport/ which omits the wind and ssh of Fig. (1). The eddy variability is very large, and will leave you wondering if a concise and simple description of the circulation is possible. The eddy variability of the upper ocean transport (upper 400 m) is a little less so: https://www2.whoi.edu/staff/jprice/as-uotransport/

- **Baroclinic wave:** The flow in a baroclinic wave is surface-intensified and bidirectional (Sec. 4.7, Part 4). The upper ocean transport may be substantial, but compensated by a transport of equal magnitude and opposite direction in the deep ocean so that the total transport vanishes. [8]

Estimating volume transport via a pseudo-streamfunction

The amplitude of a circulation is often best represented by the volume transport, $\mathbf{M} \times width$ [m^3 sec^{-1}], or via a (pseudo-)streamfunction,

$$\Psi(x)^{ann} \; = \; -\int_{India}^{x} {}^{y}M(x,\, y_o)^{\,ann}\, dx, \tag{1}$$

where y_o is the constant latitude equivalent. In the cases considered here, the starting point of the integration is the west coast of India where $\Psi = 0$, and integration proceeds westward (the usual convention for ocean circulation studies). The ${}^{y}M$ may be time-averaged over the record length or a composite average over a specific season, e.g., all of the summers to give $\Psi(x)^{sum}$. Alternatively, if the transport is summed over the upper 400 m only, then the notation for the winter composite average is

$${}_{uo}\Psi(x,t)^{win} \; = \; \int_{Somalia}^{x} {}^{y}_{uo}M(x,\, y_o)^{win}\, dx. \tag{2}$$

These Ψs are said to be pseudo-streamfunctions because the vector field ${}_{uo}\mathbf{M}(x,y,t)$ is not strictly incompressible and so in general, ${}^{x}M \neq \partial\Psi/\partial y$. Nevertheless, the Ψs are well-defined and meaningful when taken on their own.

Local, basinwide, and remote wind forcing.

The relationship between wind forcing and the ocean circulation at a given point may be characterized as one or several of

- **Local:** The Sverdrup relation is local in that the meridional transport at a point is attributable to the wind stress curl at that point, and nothing more. Ekman transport is also local.
- **Basinwide:** A classical western boundary current is a basinwide, wind-driven phenomenon, insofar as its amplitude will depend upon the wind stress curl over the full span of the basin to the east (and not just the local stress curl). When applied to the Arabian Sea in Sec. 6, the basin width will be replaced by the scale of the wind stress, but the fundamental idea holds. Some authors refer to this as a 'nonlocal' relationship, and others refer to it as 'remote'. Either usage is sensible, but here remote will be reserved for something that is both very distant and only incidentally connected to the basin winds.

[8] Any given current profile is likely to be a superposition of these two archetypes. A case can be made for investigating two shallower vertical integration intervals. A surface layer O(50 m) thick, would be weighted much more towards Ekman transport. The sea surface, or shallowest possible level, is of greatest practical importance and is also the most readily observed (Beal et al., 2010[14]). The intent here is to be concise, and given that the main interest is the wind-driven, dynamic response, two depth intervals of transport is enough.

- **Remote:** An anomaly of ssh that originates within an adjoining basin may propagate to the observation site with no immediate connection to local or basinwide winds. In this case the adjoining basin is the Bay of Bengal, and wind forcing by the South Asia Monsoon appears to set the annual periodicity and the phase of the process. Nevertheless, this will be termed remote forcing, rather than remote wind forcing, since the most salient feature is the waveguide and propagation mechanism within the Arabian Sea.

3 South Asia Monsoon winds reverse with the seasons

The winds over the Arabian Sea are a part of the South Asia Monsoon system. An important feature of the surface wind field is the Intertropical Convergence Zone (ITCZ), which marks the ascending branch of the Hadley Cell. The ITCZ is a low pressure trough that encircles the globe, and is the convergence of the northeast and southeast trade winds. ITCZ weather is characterized by persistent cloud cover and often heavy precipitation. The ITCZ is generally not far from the thermal equator and so follows the sun's annual march, though with a lag of one to two months and with very large zonal perturbations caused by longitudinal variation of land/sea distribution.[9] Associated with the ITCZ's annual migration, the winds over the Arabian Sea have a pronounced seasonal variation in both amplitude and direction and this in turn causes a marked seasonal variation of the Arabian Sea circulation.

3.1 Summer winds, the Southwest Monsoon

During boreal (northern hemisphere) summer, the land mass of South Asia warms well beyond the SST of the NIO, and the ITCZ migrates northward, as far as 20 N by June or July (Fig. 3). The southeast trade winds coming from the southern hemisphere are almost due north crossing the equator, and are deflected farther clockwise by the Coriolis force over the Arabian Sea. The winds to the south of the ITCZ are predominantly southwesterly (from the southwest, Figs. 3 - 5), and the summer season is often called the Southwest Monsoon. The ITCZ is somewhat localized in the meridional direction compared with the broad expanse of the high pressure (descending) side of the Hadley cell (the Mascarene or South Indian Ocean high in boreal summer), and so the passage or the arrival of the ITCZ is somewhat event-like, taking a couple of weeks, typically. In early summer, when the ITCZ is moving northward, the change in wind and weather associated with the ITCZ's northward passage is especially noteworthy and is termed the Southwest Monsoon onset. The north-south translation of the ITCZ is not smoothly sinusoidal and not well-defined by a single value, but nevertheless it will be useful later to have at least a rough idea of the translation rate, $V_{itcz} \approx$ 23 deg of latitude in 3 months $\approx$ 0.4 m sec^{-1}.

[9] Gadgil, S. (2003) The Indian monsoon and its variability, Ann. Rev. of Earth Planet. Sci., 31:429-467. doi: 10.1146/annurev.earth.31.100901.141251

By midsummer, when the ITCZ is established over the northern Arabian Sea and Northern India and Pakistan, the Southwest Monsoon has some of the character of a large scale land-sea breeze — a thermally direct circulation driven by the large temperature difference between the comparatively cool Arabian Sea and the very warm land mass of the Indian subcontinent.[10] Strong southwest winds with stress up to 0.5 Pa prevail over most of the basin. The Southwest Monsoon winds have a local maximum about 400 km offshore known as the Findlater Jet.[11] Along 10 N, the jet axis is typically near 55 E. This jet structure of the wind field gives the wind stress curl two signs over the Arabian Sea: there is negative stress curl over most of the central Arabian Sea, up to -6 $\times 10^{-7}$ Pa m^{-1} (Fig. 5), with largest values on the western side of the basin, there is a sign reversal on the axis of the Findlater Jet, and very large, positive stress curl, up to 8 $\times 10^{-7}$ Pa m^{-1}, within a few hundred kilometers adjacent to the western coast.[12] As discussed in Secs. 4 and 5, the somewhat intricate horizontal structure of the Southwest Monsoon wind stress curl makes a clear imprint onto the summertime, meridional volume transport. By comparison, the correlation between wind stress curl and meridional transport is much less clear during the wintertime, Northeast Monsoon season.

3.2 Winter winds, the Northeast Monsoon

During the boreal winter, the land mass of South and Central Asia is much cooler than the SST of the Indian Ocean and the ITCZ is at about 8 S over the South Indian Ocean. The descending branch of the Hadley cell over Central Asia (Mongolian/Siberian High) sets up a flow of dry continental air from northeast to southwest over the Arabian Sea (Fig. 4 upper), and ultimately into the low pressure trough of the ITCZ. This is called the Northeast Monsoon. The associated wind stress over the open Arabian Sea is

[10] The sun's annual march across the sky is the essential cause of seasonality, including the South Asia monsoon and the annual migration of the ITCZ, and yet the timing and the rate of the ITCZ passage and monsoon wind reversals do not exhibit the kind of smoothly sinusoidal, astronomical regularity that this implies. Rather, the ITCZ moves quickly between winter and summer modes, spending comparatively little time over the equator. As well, the ITCZ is embedded within the irregular hemispheric-scale weather associated with a meandering jet stream, the El Nino/Southern oscillation, and Madden-Julian oscillations, among others, with the result being considerable year-to-year variation in the rate and amplitude of the Southwest Monsoon onset. For much more on the ITCZ, see the review by Schneider, T., T. Bischoff and G.H. Haug (2014), Migrations and dynamics of the intertropical convergence zone, Nature, 513, 45-53, and an excellent web site, https://climate-dynamics.org/why-does-the-itcz-shift-and-how/

[11] The Findlater Jet has a maximum at an altitude of only about 1.5 km above sea level, and so is steered by the mountainous topography of East Africa and Madagascar. It is often likened to an oceanic western boundary current. One of the pioneering papers on this phenomenon is highly recommended, Findlater, J. (1969), A major low-level air current near the Indian Ocean during the northern summer. Q J Royal Met. Soc., 95, 362-380.

[12] Other estimates of wind stress and wind stress curl may be found in Schott and McCreary (2001)[1] and by Halpern, D., M. H. Freilich, and R. A. Weller, (1998), Arabian Sea surface winds and ocean transports determined from ERS-1 scatterometer. J. Geophys. Res., 103, 7799-7805.

moderate, about 0.1 Pa, and varies spatially from northwest to southeast. The strongest northeast winds are on the western side of the basin; along 10 N, the maximum is typically about 400 km offshore (Fig. 5). The curl of the wind stress is positive over most of the Arabian Sea and modest amplitude, about 0.5×10^{-7} Pa m^{-1}, and large and negative, up to -3×10^{-7} Pa m^{-1}, over a several hundred kilometer wide region adjacent to the western boundary.

4 Arabian Sea circulation varies strongly with the seasons

The most compelling aspect of NIO and Arabian Sea oceanography is the marked seasonality of the winds and the ocean circulation. But not everything changes with the seasons. The relative high of ssh within the comparatively fresh Bay of Bengal and the relative low ssh within the salty Persian Gulf and Gulf of Aden persist year-round (Fig. 2). These essentially thermohaline properties owe to regional climate: high river runoff and high precipitation over Southeast Asia, and strong evaporation in excess of precipitation over Southwest Asia.

4.1 Summertime ssh and circulation

The major feature of the ensemble-averaged, summertime ssh is a compact, high pressure anticyclonic gyre centered on about 10 N, 60 E (Fig. 2, lower). The ssh amplitude is modest, about 0.4 m, (Fig. 7, upper) but significant at this tropical latitude. In the smoothed AVISO ssh, this high appears to be a more or less single feature. There is a hint of a Great Whirl at 8 N, 52 E, which is a very vigorous feature of the real ocean. In the less heavily smoothed SODA ssh (Fig. 4, lower), this anticyclonic gyre appears to be a collection of three anticyclonic eddies, GW, SE and SEII, about which more in Sec. 4.2.

The most dramatic and most remarked-upon aspect of the summertime Arabian Sea circulation (Fig. 4) is a strong, upper ocean flow to the northeast along the coast of Somalia and Oman, the Somali Current (east of Oman, this is also called the East Arabian Current). This western boundary current appears in early summer, usually within a few weeks after the onset of the Southwest Monsoon winds. The timing depends upon the location along the western boundary, and varies from year to year, as does the onset of the Southwest Monsoon wind. In situ observations[1] show that the fully-developed, Southwest Monsoon Somali Current has a near-surface speed that can exceed 2 m sec^{-1}, a depth (e-folding) of about 300 m, (Fig. 8), and a volume transport of roughly 30 Sv, (though with some estimates considerably higher). The summertime Somali Current is thus comparable in speed and volume transport to several of the semi-permanent western boundary currents of Table 1.

To make a quantitative estimate of the Arabian Sea circulation it will be helpful to define a control volume that has a simple but interesting configuration: all of the Arabian Sea north of 10 N latitude, and extending from the sea surface to the sea floor, Fig. (4). This bounding southern latitude is arbitrary, but has the advantage that it intersects land on both ends, and is more or less midway between the Great Whirl and the island of Socotra. As noted above, 10 N does cut through the Socotra Eddy and SEII,

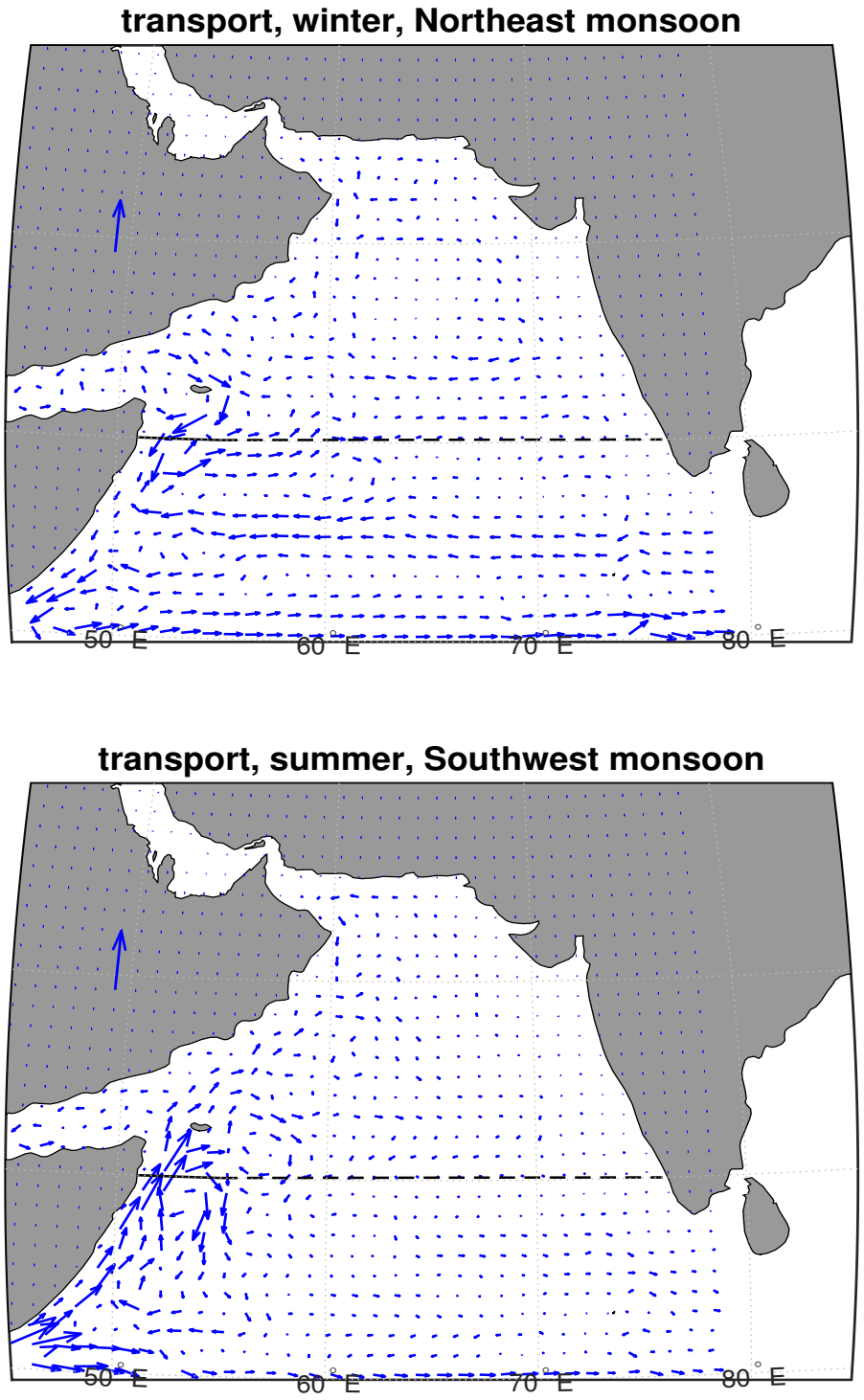

Figure 6: Transport (volume transport per unit width) computed from SODA reanalysis ocean currents integrated over the full water column and then composite averaged over the **(upper)** winter, $\mathbf{M}(x,y)^{win}$, and over the **(lower)** summer, $\mathbf{M}(x,y)^{sum}$, 1990 - 2010. The isolated vector over the Arabian peninsula has an amplitude of 250 m^2 sec^{-1}. The black line along 10 N is the open, southern boundary of a control volume used to evaluate meridional volume transport discussed in Sec. 5. The pronounced seasonality of the Somali Current is clearly evident here, as are the summertime Great Whirl centered on 8 N, 53 E, and the Socotra Eddy at about 11 N, 57 E, cf. Fig. (4), lower.

which are evident in several of the analyses. There are two mediterranean basins on the western and northern side of the Arabian Sea (Red Sea/Gulf of Aden and Persian Gulf/Gulf of Oman, Fig. 3) that inject distinctive, warm and saline water masses into the thermocline, but not a substantial volume flux. Hence the western, northern and eastern boundaries of this Arabian Sea control volume are effectively impermeable (no normal flow) coastlines, while the southern boundary along 10 N is completely open. To define the Arabian Sea circulation we will first seek to describe *where* and *when* there is meridional flow across the 10 N boundary in Secs. (4) and (5), and then seek to explain *why* there is meridional flow in Sec. (6).

The integration (1) that evaluates the streamfunction can be continued all the way from India to the western boundary on the coast of Somalia to give just one number, the net volume transport across 10 N. The streamfunction returns very close to its presumed starting value, 0, at the western boundary (Fig. 7, lower). This is to be expected on a physical basis, assuming that there is no significant secular trend of sea level, i.e., that the volume of sea water within the control volume is effectively constant. The inference is that the sampling in depth and longitude of the SODA ocean currents gives a reasonably well-resolved volume transport across the 10 N section.

The annual mean streamfunction (the black line of Fig. 7, upper) shows a modest flow to the south over most of the basin, reaching a maximum of about 5 - 10 Sv, and a fairly narrow flow to the north near the western boundary. More interesting is the seasonality of the transport, here defined over the summertime Southwest Monsoon period, the composite average over June, July and August (the red line of Fig. 7) and a wintertime Northeast Monsoon, the composite average over December, January and February (the blue line). These are dramatically different, as the maps of seasonally-averaged transport and ssh imply they should be, cf. Fig. (6).

The summertime streamfunction indicates southward transport over the interior, 75 E to 55 E, with a maximum of about 30 Sv to the south. The upper ocean transport is just slightly less, indicating that the vertical structure is approximately equivalent barotropic, and implying wind-driven flow. Farther west, the streamfunction goes rapidly to zero on the western boundary, indicating a northward volume transport of the same magnitude within a fairly narrow western boundary region. The narrow width of this northward flow implies a rapid current — the Southwest Monsoon season Somali Current, which is readily apparent in the transport map of Fig. (4), lower. The summertime ssh profile across 10 N thus displays a pattern like that of the North Atlantic subtropical gyre, a fairly narrow region of large positive slope on the west side of the basin associated with the rapid, north-eastward flowing Somali Current, and a more gradual negative slope over the basin interior suggesting southward geostrophic flow in the upper ocean (Fig. 7, lower). The corresponding ssh amplitude is about 40 cm, noted above. The interior, southward flow of the Southwest Monsoon season isn't usually considered to be part of a named current, but as shown below, it has a magnitude consistent with the overlying negative wind stress curl and the Sverdrup relation.

The upshot is that the Somali Current appears to be the western boundary current of a basin-scale, anti-cyclonic gyre that is well-established for a few months during the summer Southwest Monsoon season, but not during the winter, Sec. 4.3.

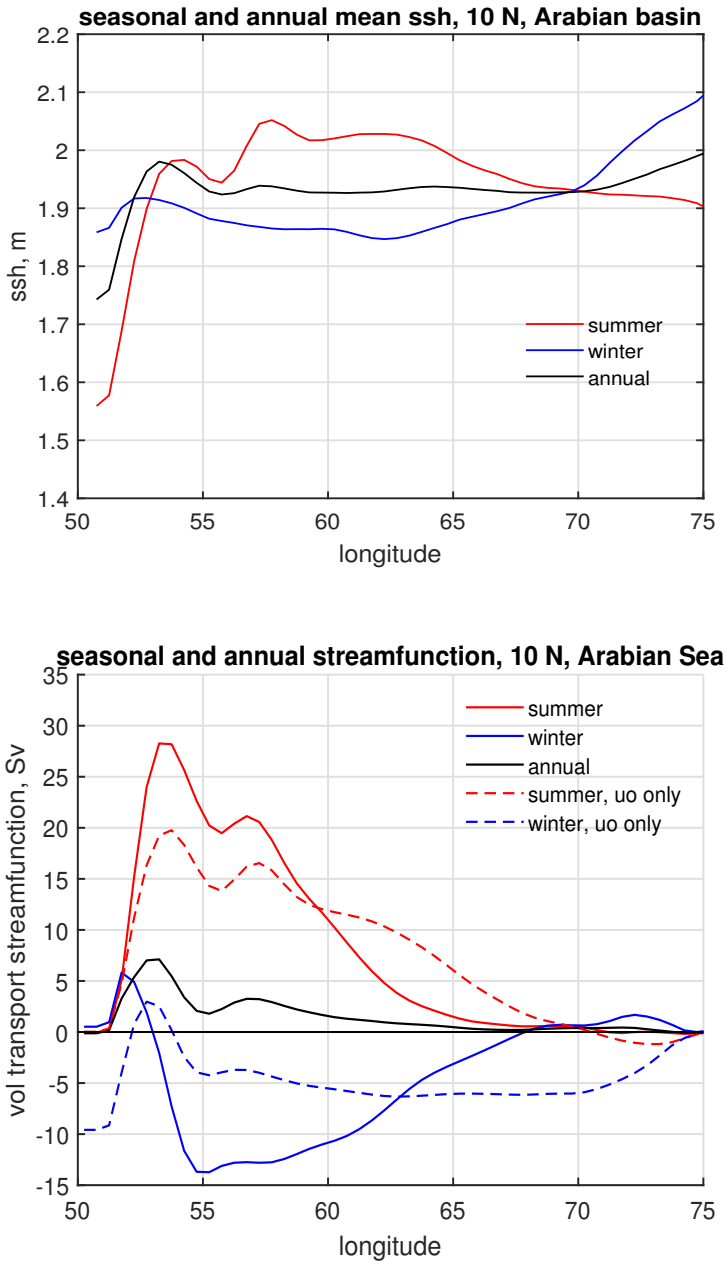

Figure 7: **(upper)** Sea surface height along 10 N in the Arabian Sea for annual mean (black) and for composite-average summer and winter (red and blue). These were computed over about 20 years of satellite altimetry complied by the AVISO project. **(lower)** Transport streamfunction computed from seasonal mean meridional velocity from twenty years of SODA reanalysis. Seasons are coded by color. The integration started on the eastern side of the basin and continued to the coast on the western side. Thus the streamfunction starts at zero and should return to zero if the net transport vanishes, which it nearly does. The dashed lines are the volume transport within the upper 400 m only. These need not return to zero on the western side of the basin. Notice the small bump in the summer streamfunction near 57 E, and also in ssh. This appears to be the composite-average signature of the Socotra Eddy.

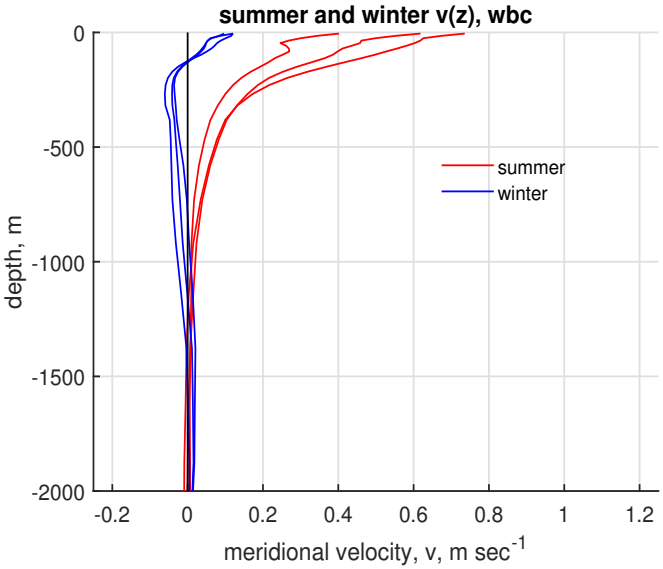

Figure 8: Profiles of the monthly mean of meridional velocity within the western boundary current on 10 N from SODA reanalysis data. Notice that the surface current in the western boundary region is northward during the summer and the winter and hence the surface current at this site does not reverse with the seasons. The volume transport does reverse, though is comparatively weak in the winter.

4.2 The Great Whirl and lesser eddies

During the summertime Southwest Monsoon season, an ensemble average of transport will show a northeastward-flowing Somali Current along the coast of Somalia and Oman up to about 20 N (Fig. 6, lower). This gives the impression that a summertime Somali Current is present instantaneously along almost the entire western boundary, and that a parcel released along the coast of Somalia would travel quickly and smoothly along a continuous trajectory all the way to the northern Arabian Sea, as if in a laminar flow. Probably not; direct evidence from drifter trajectories[13] and from monthly maps of transport[7] is that the Somali Current is frequently disrupted by large amplitude eddies and meanders. Indeed, the Arabian Sea is as eddy-rich and chaotic as any mid-latitude basin, and moreover, some of the eddies are large and intense.

An especially impressive eddy is the high pressure anticyclone that appears regularly in summertime near 8 N, 53 E (Figs. 4, lower, and 6, lower). This feature was recognized long ago and dubbed, fittingly, the Great Whirl.[14] In most years the Great Whirl forms in late spring when and where the 6 N ridge intersects the western boundary of the Arabian Sea and forms a small, pinched off, anticyclonic loop.

[13] A comprehensive, modern, data-based analysis of the annual variation of the near-surface circulation is by Beal, L. M., V. Hormann, R. Lumpkin and G. R. Foltz, 2013, Journal of Physical Oceanography, The response of the surface circulation of the Arabian Sea to monsoonal forcing. 43, 2008 - 2022. For North Indian Ocean eddies see Trott, C. B., Subrahmanyam, B., Chaigneau, A., and Roman-Stork, H. L. (2019). Eddy-induced temperature and salinity variability in the Arabian Sea. Geophysical Research Letters, 46, 2734 2742. https://doi.org/10.1029/2018GL081605.

[14] Excellent discussions of the Great Whirl are by Beal, L. M., and Donohue, K. A. (2013). The Great Whirl: Observations of its seasonal development and interannual variability. Journal of Geophysical Research: Oceans, 118, 1 13. https://doi.org/10.1029/2012JC008198, and by Melzer, B. A., Jensen, T. G., and Rydbeck, A. V. (2019). Evolution of the Great Whirl using an altimetry-based eddy tracking algorithm. Geophysical Research Letters, 46, 43784385. https://doi.org/10.1029/2018GL081781

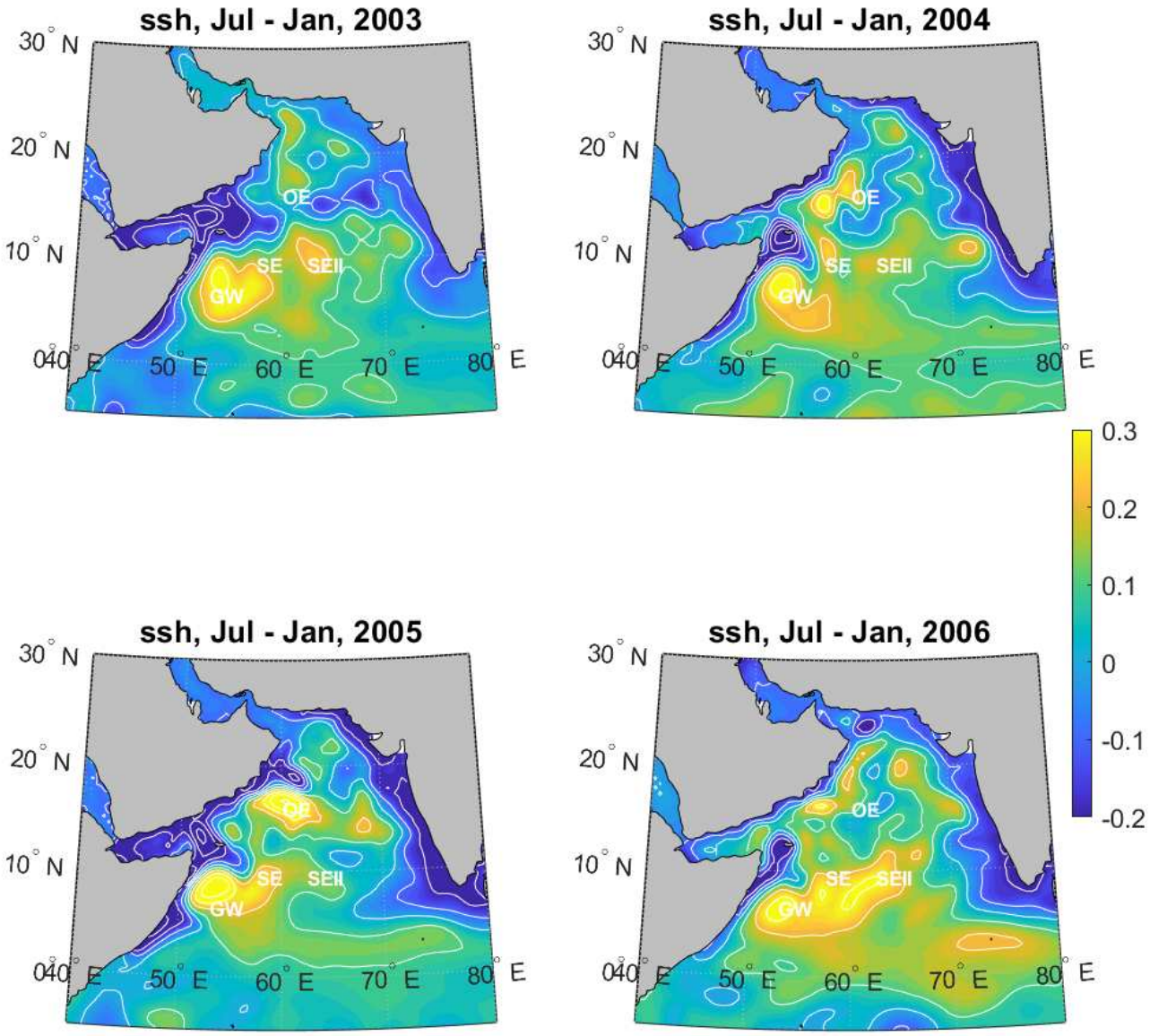

Figure 9: Snapshots of ssh in July - ssh in January, for four successive years, 2003 - 2007. The anticyclonic gyre is a roughly 1500 x 1500 km relative high centered on about 9 N, 62 E. Notice that the northern half of the gyre is very lumpy; you could argue that the gyre is nothing more than a small handful of anti-cyclonic eddies. The largest and most regular of these is the Great Whirl, GW, usually at about 8 N, 53 E. Three other eddies that are apparent in the ensemble mean ssh are the Socotra Eddy, SE, its neighbor, SEII, and the Omani Eddy, OE. The GW and SE are widely recognized in the literature; SEII and OE are not.

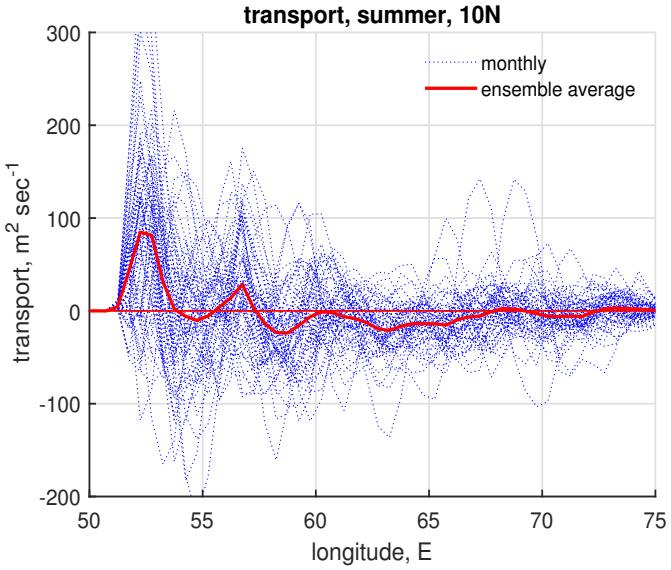

Figure 10: Meridional transport across 10 N for each summer month between 1990 and 2010 (60 samples). The thicker red line is the summer ensemble average. The month-to-month variability is very large, and any one transport estimate might look nothing like the ensemble mean.

The amplitude increases rapidly, apparently in response to the Southwest Monsoon winds, and by midsummer the Great Whirl has a diameter of about 300-400 km, which is about three times the baroclinic radius of deformation, and an azimuthal transport that is comparable to that of the Somali Current. It is noteworthy that the initial formation of the Great Whirl appears to be a matter of remote forcing by internal, mesoscale ocean dynamics, mainly, rather than the local and basin-wide wind stress curl/Sverdrup transport relationship that will be emphasized in most of what follows. The Great Whirl disappears not long after the Southwest Monsoon winds die out in the fall.

The Great Whirl remains mostly to the south of the 10 N section that will be of particular interest here (the dashed black line of Fig. (4), discussed next). However, there is another high pressure, anticyclone, the Socotra Eddy (SE), that is squarely in our sights. The Socotra Eddy is typically centered near 11 N, 57 E, and is comparable in size to the Great Whirl, but about half or a third as intense, judging from its ssh signature in Fig. (4). The Great Whirl and the Socotra Eddy are widely recognized as significant features of the Arabian Sea. Putting names on still other eddies would seem to be (and might actually be) a frivolous and unproductive endeavor, but, there is evidence in the summer ensemble mean ssh (Fig. 4) of two additional anticyclones that are fairly prominent in many years, and that will be mentioned again later (and evident also in the hydrographic data studied by Bruce[1]). One of these is an eastern neighbor of the Socotra Eddy, centered on about 12 N, 61 E. This eddy appears to be similar overall to the Socotra Eddy, though usually not as strong or as symmetric, and so SEII seems appropriate (Fig. 9). The fourth eddy is an anticyclone centered on about 18 N and 61 E, the northern edge of the gyre and just offshore of Oman; Omani Eddy, or OE seems appropriate. This eddy is coincident with a local maximum of negative wind stress curl that is noted below.

All of these eddies are seasonal, appearing in summer and disappearing in winter. Given this clear-cut seasonality, it appears that these eddies are wind-driven, though perhaps only indirectly via

instability of the gyre. At least GW and SE can be simulated by a fairly simple (one layer, reduced gravity) model provided with realistic basin geometry and realistic, seasonally varying winds.[15] These features are referred to as 'eddies' solely because of their sub-basin horizontal scale and roughly circular planform. However, a good case can be made for calling them 'gyres' insofar as they appear to be wind-driven and deterministic in that they repeat from year to year, though of course with some variation. Collectively, these eddies make up a significant fraction of the basin-scale anti-cyclonic gyre (a subjective judgment) and so the distinction between gyre and eddy is significantly blurred in the Arabian Sea.[16]

4.3 Wintertime ssh and circulation; remote forcing from the Bay of Bengal

During winter, the ssh over the central and western Arabian Sea is almost featureless, at least in the smoothed and averaged AVISO ssh of Fig. (2), upper. There is a weak, relative low, only about 5 - 10 cm, compared to the western boundary region, which is not inconsistent with the weak, mostly positive stress curl of the wintertime, Northeast monsoon. There is somewhat higher ssh evident in the eastern and southern part of the Arabian Sea, roughly 30 cm compared to the center. This high ssh appears to have an origin in the relatively fresh Bay of Bengal, where sea level is on average about 40 cm higher than in the saltier Arabian Sea. The Bay of Bengal is also subject to the South Asia Monsoon. During the Southwest Monsoon winds of summer, the ssh near the southern tip of India and Sri Lanka is somewhat lower than over most of the Bay of Bengal (Fig. 2, lower). During the winter, when the wind comes from the northeast, the characteristic high ssh of the Bay of Bengal fills in all the way south to Sri Lanka, and then appears to spread around the southern tip of India and Sri Lanka beginning in early winter (the orange and yellow wedge of high ssh on the southeastern side of the Arabian Sea in Fig. 4, upper and Fig. 2, upper). High ssh then spreads into the Arabian Sea along two axes: northward along the eastern coastal boundary (west coast of India) as a coastal Kelvin wave, and westward in a several hundred kilometer wide ridge that is centered on roughly 6 N latitude. Beginning in early to mid-winter, the 6 N ridge begins to extend (propagate) westward at about the speed expected of a low mode, baroclinic Rossby wave, a few 10s of km per day at this latitude, and thus crosses the Arabian Sea basin in O(100 days).[17]

The slope of ssh over the wintertime Arabian Sea is dominated by the coastal high and the 6 N ridge, but notice that there is little obvious, corresponding signature within the field of the total transport, cf. Fig. (6, upper). To detect the ocean current signature of the 6 N ridge, and specifically the meridional current, it is helpful to evaluate the pseudo-streamfunctions along 6 N latitude, $\Psi(x,t)^{win}$ (the solid blue line of Fig. 11, lower) and the upper-ocean version, ${}_{uo}\Psi(x,t)^{win}$ (the dashed blue line). These are just like Eqns.

[15] Luther, M. E., and J. J. O'Brien (1985) A model of the seasonal circulation in the Arabian Sea forced by observed winds. Prog. Oceanogr., 14, 353-385, and recently by Wang et al. (2018)[2].

[16] Compare this with the North Atlantic subtropical gyre of Figs. 1 - 3. Given sufficient temporal averaging on hydrographic data, several decades, North Atlantic mesoscale eddies largely disappear leaving behind a smoothly varying, large-scale, time-mean subtropical gyre.

[17] This description is merely what can be seen in the ssh field. For a much more complete treatment see Yu, L., J. J. OBrien and J. Yang (1991) On the remote forcing of the circulation in the Bay of Bengal, J. Geophys. Res. Oceans, 96, C11, 449-454 and Shankar, D., and S. H. Shetye (1997) On the dynamics of Lakshadweep high and low in the southeastern Arabian Sea. J. Geophys. Res-Oceans, 102, C6, 12,551 - 12,562. More recent is Wang et al., (2018)[2].

(1) and (2) except for the latitude. The ${}_{uo}\Psi(x)^{win}$ shows a significant signal of northward, meridional, upper ocean transport between about 55 E and 70 E (also in Fig. 1 and the animation linked there), coincident with the western leading edge of the 6 N ridge, cf., the ssh of Fig. (11), upper. The amplitude of the northward volume transport is about 12 Sv. There is little or no sign of this in the total transport. This is additional evidence, along with the westward propagation rate, that the remote forcing that comes from the Bay of Bengal (the 6 N ridge) may be characterized as a free, baroclinic Rossby wave.

Within the western third of the basin (west of 60 E) the streamfunctions along 6 N and 10 N reveal a different pattern. The total transport and the upper ocean transport are in the same direction and have comparable magnitudes. This suggests a mainly wind-driven flow very near the western boundary having a magnitude of about 10 Sv, and which is also referred to as the Somali Current. There is a comparable northward flow a few hundred kilometers offshore. The wintertime Somali Current is quite variable in time and space (Fig. 6, upper) and even on ensemble average, there is little suggestion of a continuous western boundary current. The wintertime ssh has a similar character, i.e., small amplitude and somewhat indistinct pattern on the basin scale. The Arabian Sea circulation doesn't so much 'reverse' with the seasons, which implies symmetry in the winter and summer amplitudes, but rather it 'varies' seasonally, and by quite a lot.

5 Sverdrup transport is correlated with the summertime, meridional transport

You may have noticed that there is at least a qualitative consistency between the mainly negative wind stress curl over the basin interior during summer, and the Sverdrup expectation of an anticyclonic gyre and poleward western boundary current during summer (noted by Bruce, 1983[1]). That suggests that it might be fruitful to evaluate the Sverdrup relation quantitatively, and define where and when it succeeds (summer), and just as important, where and when it fails (winter). To do this, take the wind stress curl used to make Fig. (5) and evaluate the Sverdrup streamfunction,

$$S(x)^{ann} = \frac{-1}{\rho\beta}\int_{India}^{x} \overline{\nabla\times\tau(x,y_o,t)}^{\,ann}\, dx, \tag{3}$$

where the time average can be the annual mean (the black line of Fig. 12) or over a given season (red and blue lines) and y_o is 10 N equivalent. The Sverdrup streamfunction predicts rather weak and indistinct transport on annual mean and during winter (signs are reversed between these two). There is significant meridional Sverdrup transport during the summer, approx. 27 Sv southward over the interior, i.e., east of about 55 E. This may be compared to the meridional transport streamfunction, (Fig. 7), which indicates about 30 Sv southward during the summer over the basin interior. From this first look, it appears that the time-independent Sverdrup relation gives a fairly good account of the amplitude of the summer, Southwest Monsoon season, meridional transport found in the interior of the Arabian Sea at 10 N (and, it should be noted, within the SODA reanalysis). This does not hold during the wintertime Northeast Monsoon, when the Sverdrup estimate has the correct sign, but considerably smaller magnitude compared to the actual meridional transport.

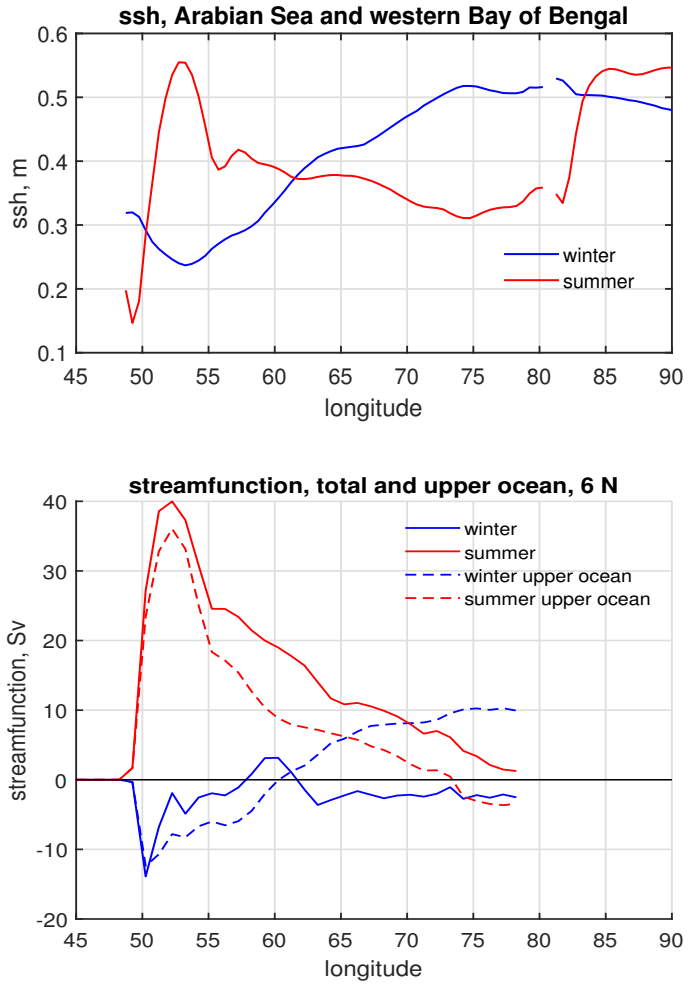

Figure 11: A zonal section along 6 N. **(upper)** The ssh along 6 N from the coast of Somalia to the western Bay of Bengal. Summer composite average (red) and winter (blue). The small gap at about 81 E is the southern tip of Sri Lanka. These are composite averages over 20 years. **(lower)** The composite-averaged streamfunctions $\Psi(x,t)$ and ${}_{uo}\Psi(x,t)$ Eqn. (2) evaluated along 6 N. **(lower)** The total transport and upper ocean transport are fairly similar during the summer (compare the red solid and red dashed lines) suggesting equivalent barotropic flow. They are quite different during winter (blue solid and dashed lines), especially in the eastern half of the basin. The northward upper ocean transport is coincident with the positive ssh slope on the western side of the 6 N ridge, cf. the blue line of the upper panel.

5.1 Regional, seasonal Sverdrup transport

There is nothing special about 10 N insofar as the Sverdrup relation is concerned, and so it should be just as appropriate to compare the Sverdrup transport $S(x,y)$ to the meridional transport ${}^{y}M(x,y)$ throughout the Arabian Sea — Figs. (14) and (13) are for winter and summer. The Sverdrup transport is mapped even at locations immediately adjacent to a zonal boundary, as in the narrow and shallow Gulf of Aden, where a significant meridional transport is not expected or observed.

Wintertime. It has already noted that the wintertime meridional transport and Sverdrup transport are not consistent along 10 N, and this presentation is no different; ${}^{y}M(x,y)^{win}$ and $S(x,y)^{win}$ display fairly small scale, and generally low amplitude features that are evidently not correlated.

Summertime. With some allowance for the obvious, unphysical features in the S^{sum} field noted above,

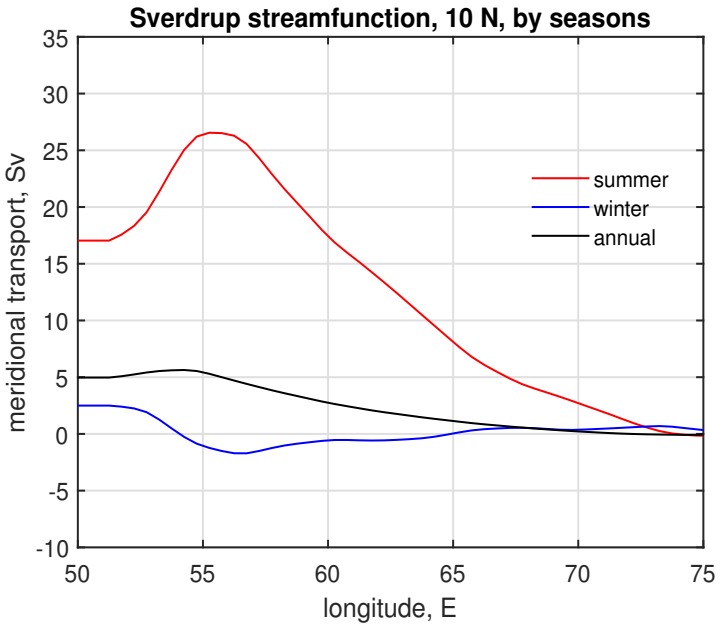

Figure 12: The Sverdrup transport streamfunction computed from the annual and seasonal mean wind stress curl Fig. (5) via Eqn. (3). Seasons are coded by color. The integration started on the eastern side of the basin and continued to the coast on the western side. Thus the streamfunction starts at zero, but as we noted in Sec. 6, Part 4, the Sverdrup streamfunction need not and in this case does not return to zero on the opposite coast. The summertime Sverdrup streamfunction (red line) compares reasonably well with the streamfunction computed from meridional velocity, the red line of Fig. (7), in the region east between about 56 E and the coast of India, i.e., the interior, but not in the western boundary region. During the winter, Sverdrup streamfunction (the blue line) does not compare well with the streamfunction computed from meridional velocity, cf. the blue line of Fig. (7).

the basin-scale distributions of ${}^{y}M(x,y)^{sum}$ and $S(x,y)^{sum}$ are fairly consistent in showing three broad regions based upon the sign of ${}^{y}M^{sum}$.

- Eastern boundary region. Within a few hundred kilometers of the eastern side of the basin (west coast of India) there is fairly low amplitude, mostly positive (northward) ${}^{y}M^{sum}$, as well as mostly positive S^{sum} of comparable, small magnitude. This is a region where one would expect significant influence of remote forcing from the Bay of Bengal,[1], and all that will be added here is that local wind forcing in the Sverdrup sense might be of some importance as well.

- Central basin. Over the central region of the Arabian Sea, the transport ${}^{y}M^{sum}$ is negative (southward) Fig. (13) associated with the eastern side of the Findlater Jet noted in the discussion of the wind field. Larger values are found towards the western side of the basin (but not directly adjacent to the western boundary, discussed below). There is roughly comparable negative S throughout the central part of the basin, and including the occurrence of larger values in the

western third of the basin, so that there is a fairly convincing correlation of S^{sum} with ${}^{y}M^{sum}$ on the basin scale. This correlation would be expected if the Sverdrup relation was relevant.

There appears to be a correlation of stress curl and meridional transport within the central basin on somewhat shorter scales, O(300) km. One interesting feature is the local maximum of stress curl and transport at the northern end of the gyre, roughly 18 N, 62 E, which is the site of the so-called Omani Eddy (Fig. 3). In fact, it is no great exaggeration to say that the Omani Eddy *is* most of the gyre at this latitude. There are also more or less coincident maxima at 11 N, 63 E, the Socotra Eddy, and at 13 N, 70 E, the site of the SEII eddy. This visual correlation suggests that these eddies may be, in part, a result of the local wind stress curl.[18]

- Western boundary region. The region immediately adjacent to the western boundary is important and interesting. The ${}^{y}M^{sum}$ field is strongly positive (northward) close to the western boundary, with an amplitude up to 200 m^2 sec^{-1} (cf. Fig. 13, lower) in some places, and well beyond the color range of the figure. This is, of course, the region of the summertime Somali Current and so very large ${}^{y}M^{sum}$ is expected. The Sverdrup transport also has very large positive values in a nearly coincident region along the coast. The values of the Sverdrup transport are, however, considerably less than the meridional transport, the maximum values are roughly $S^{sum} \approx 50$ m^2 sec^{-1}. If, as suggested earlier, the summertime Somali Current can be seen as a western boundary current that returns the interior, southward Sverdrup transport back to the north, then the western boundary transport need not have any relation to the local Sverdrup transport, as occurs in the central basin. Or said a little differently, the western boundary region is more likely to have a basinwide relationship to the wind stress curl over the basin to the east, and only an incidental correlation to the local wind stress curl.

  In most western boundary currents, the local wind stress curl is a good deal smaller than the leading terms of the vorticity balance of the current, and so is negligible in the local dynamics of the western boundary current. However, the wind stress curl over the Somali Current is large enough, roughly 20% of βv, that it may be significant. The sense is that the positive wind stress curl will act to amplify the northward-going Somali Current that is expected from basin-wide volume conservation alone.

5.2 Monthly-varying transport across western boundary and interior regions

The SODA data are archived at monthly intervals, which should in principle allow a more finely resolved temporal view of the meridional transport across 10 N. However, some kind of spatial averaging is going to be required to suppress eddy variability. Here this is done by integrating over two segments of the 10 N boundary, a western boundary region (the solid line along 10 N in Fig. 4) extending from the Somali

[18] This is intriguing but far from definitive. The correlation is clear enough within the SODA reanalysis, but it isn't known (to me) that the small scale variability of the stress field and these two eddies are features of the real Southwest Monsoon wind and the Arabian Sea in the same way that the Findlater Jet and the Great Whirl undoubtedly are.

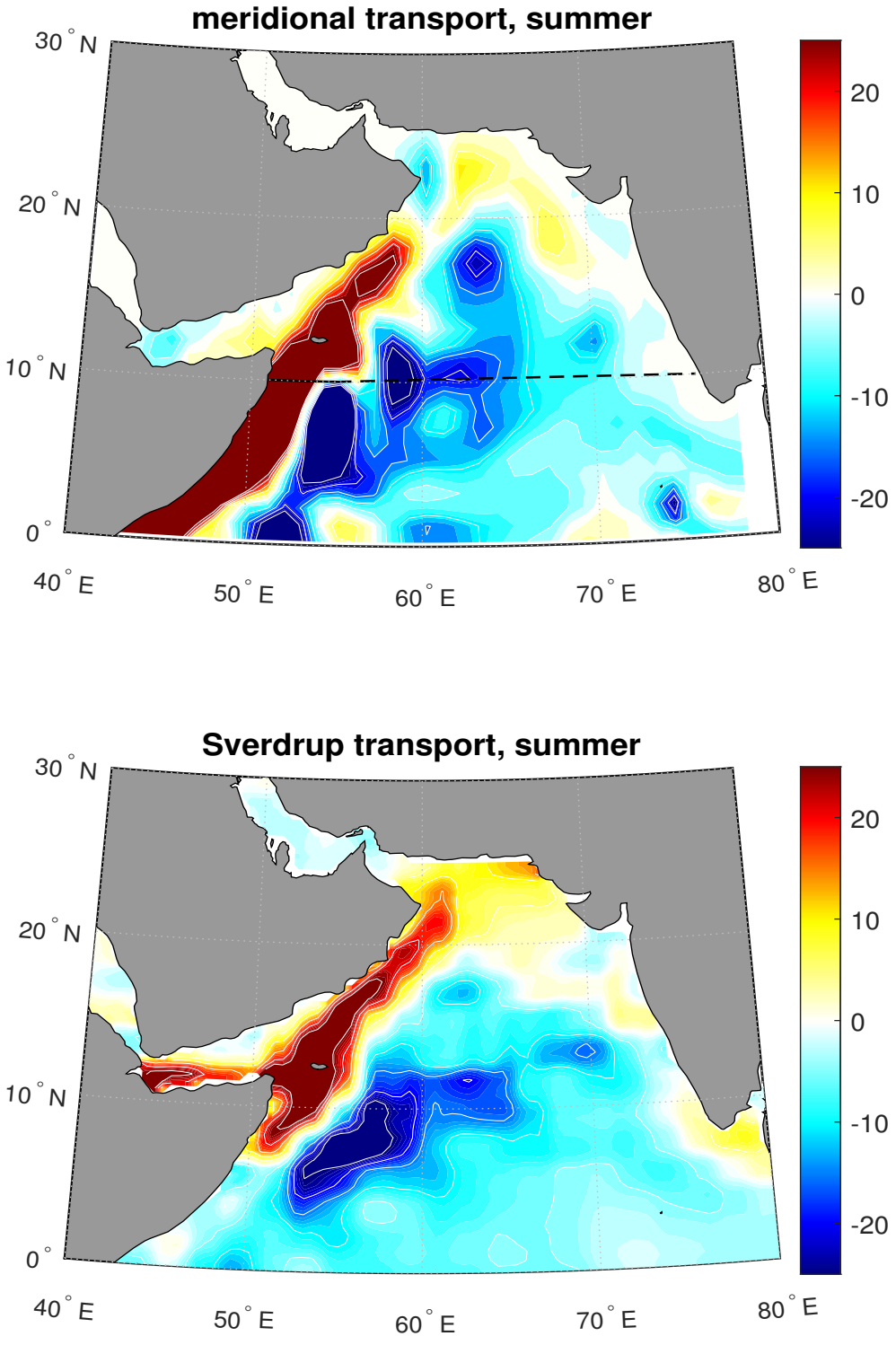

Figure 13: **(upper)** Meridional transport composite-averaged over the summer, ${}^{y}M(x,y)^{sum}$. The colorbar at right is in units m^2 sec^{-1}. The dark red region adjacent to the western boundary has some very high values, up to 200 m^2 sec^{-1}, that saturates the colorbar scale. **(lower)** Sverdrup transport, $S(x,y)^{sum}$, also composite-averaged over the summer. This figure requires considerable interpretation attempted in the main text.

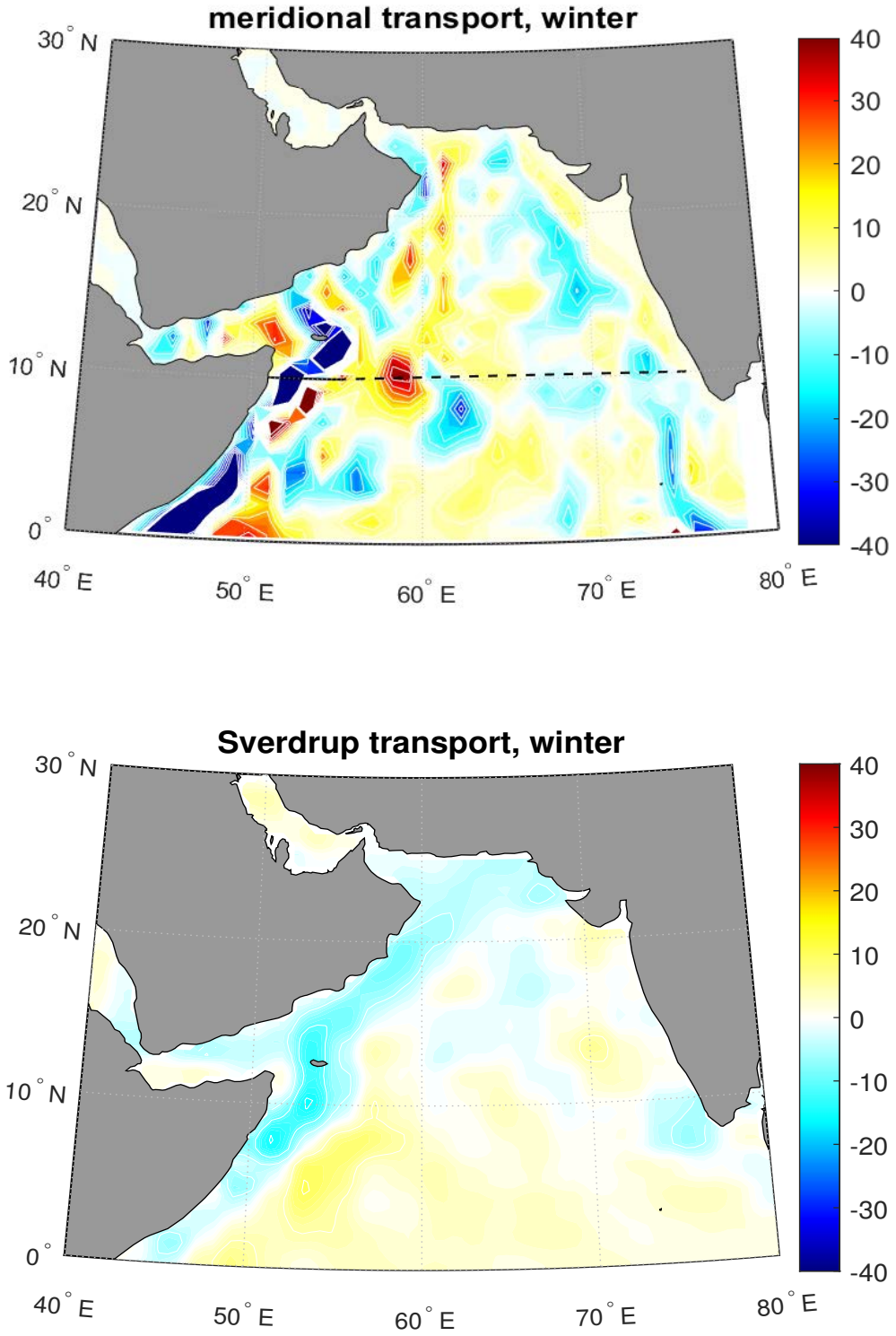

Figure 14: **(upper)** Meridional transport, ${}^{y}M(x,y)^{\,win}$, composite averaged over the winter. The colorbar at right is in units $\mathrm{m}^2\ \mathrm{sec}^{-1}$. The dark blue regions adjacent to the western boundary have high values, up to 50 $\mathrm{m}^2\ \mathrm{sec}^{-1}$, that saturate the colorbar. **(lower)** Sverdrup transport, $S(x,y)^{\,win}$, composite averaged over the winter. The generally favorable comparison of $S^{\,sum}$ with ${}^{y}M^{\,sum}$ that obtains in summer is not evident here.

coast to 55 E,

$$N(t)_{wbc} \;=\; \int_{Somalia}^{55E} {}^{y}M(x,\, y_o,\, t)\, dx,$$

and an interior region from 55 E to the coast of India (the dashed line along 10 N),

$$N(t)_{int} \;=\; \int_{55E}^{India} {}^{y}M(x,\, y_o,\, t)\, dx$$

and y_o is 10 N. This has introduced a parameter, the eastern extent of the western boundary region, 55 E, which is the Findlater Jet axis in summer (Fig. 5) and thus the longitude of zero stress curl (on average). The intent is that this N_{wbc} will represent the Somali Current, rather than the Great Whirl or the Socotra Eddy, say, but this simple-minded criterion is no guarantee of that.[19]

5.3 Sverdrup and meridional transport are highly correlated at annual and semi-annual frequencies

The monthly, meridional volume transport through these two regions shows a somewhat ragged but quite pronounced annual cycle, Fig. (15). The interior region has a southward going (negative) peak in summer, typically about 30 Sv, while the wbc region (Somali Current) has a closely comparable northward (positive) peak at the same time. The winter peak in transport is considerably smaller, about 10 Sv. It is notable that the interior transport and the wbc transport are almost exact complements, $N_{wbc} \approx -N_{int}$ whose sum, the net transport through 10 N, (the black line) is very small, $N_{wbc} + N_{int} \approx 0$, in the sense that $N_{wbc} + N_{int} \ll N_{int}$, as it should be. The same thing held for the long-term mean streamfunction, and here it is evident that conservation of volume holds also month by month. Thus the monthly transport can be represented equally well by the interior component, $N(t)_{int}$, which is unnamed and unremarked upon, or by the wbc component, $N(t)_{wbc}$, which is the justly famous Somali Current, or so intended. We will most often choose the former, given its possible connection to the Sverdrup relation.

Does the time-independent Sverdrup relation give a useful estimate of the monthly-averaged transport? On the face of it this seems unlikely, but is readily testable; evaluate $S(t)_{int}$ along the 10 N interior segment at monthly intervals,

$$S(t)_{int} \;=\; \frac{-1}{\rho\beta} \int_{India}^{55E} \nabla \times \tau(x, y_o, t)\, dx, \tag{4}$$

and compare with the corresponding meridional transport, $N(t)_{int}$ from the SODA meridional velocity. There is an obvious visual correlation between N_{int} and S_{int} (Fig. 16, upper). The auto spectra indicate

[19] You might suppose that defining and then estimating the transport of a western boundary current like the Somali Current or the Gulf Stream would be straightforward. However, in practice, there are often large, geostrophic eddies on the flank of what looks to be the main current, and so not easily distinguished from the main current, which will in any case meander significantly unless constrained by topography. The result is that the estimated transport will likely be dependent upon the criteria used to discriminate the current from the surroundings, see e.g., Heiderich, J., and Todd, R. E. (2020). Along-Stream Evolution of Gulf Stream Volume Transport, Journal of Physical Oceanography, 50(8), 2251-2270. Retrieved Sep 24, 2021, from https://journals.ametsoc.org/view/journals/phoc/50/8/jpoD190303.xml

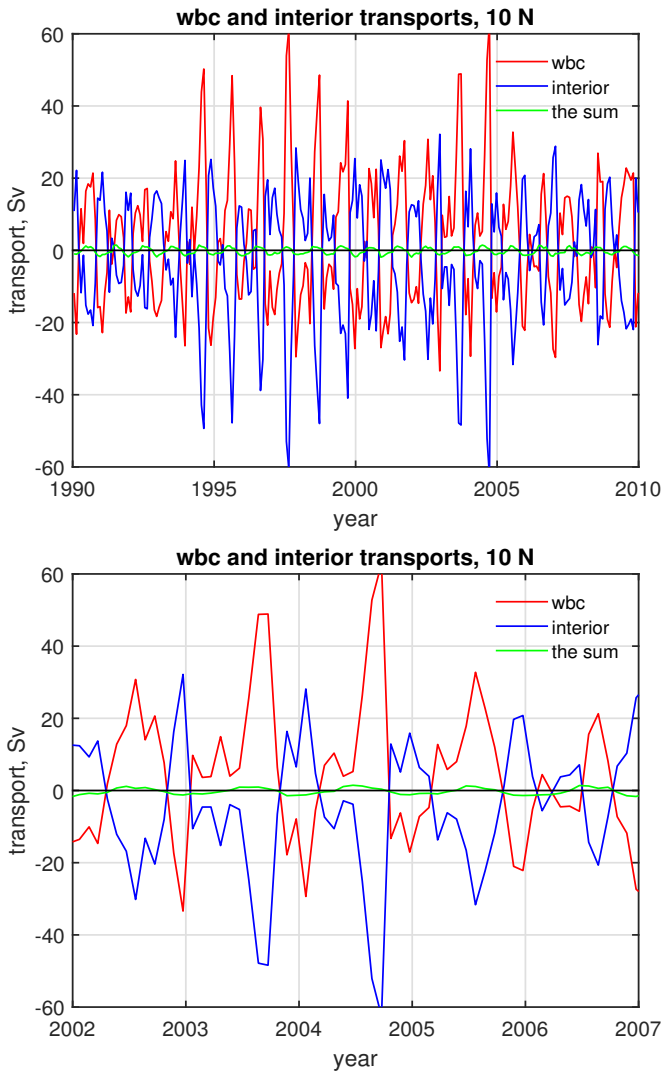

Figure 15: Volume transports across 10 N evaluated over the interior, $N(t)_{int}$ (the red line) and over the western boundary region, $N(t)_{wbc}$ (blue line). The **(upper)** panel is over two decades, 1990 - 2010, and the **(lower)** panel is a subset, 2002 - 2007. These data are from the monthly-averaged and sampled SODA 2.2.4 reanalysis and so have a somewhat spiky, unphysical appearance. Notable features are the large amplitude seasonal variation, roughly $\pm$ 30 Sv in summer, and that N_{wbc} and N_{int} are almost exact complements; their sum (the green line) is much smaller than either piece separately.

that S_{int} is a little smaller than N_{int}, roughly consistent with the the ratio of the two streamfunctions (cf., Figs. 7 and 12). The corresponding statistical measures, lagged correlation and coherence of the cross-spectra, bear out the visual impression of high correlation (Fig. 17). The maximum of the lagged correlation is approx. 0.8. The asymmetry suggests a small phase difference, with the volume transport lagging the Sverdrup transport by about two weeks. The cross-spectral coherence (frequency domain analysis) is similar; the coherence ≥ 0.9 at the annual frequency and the phase difference at the annual frequency is very small (Fig. 17, center). These results indicate that the monthly-varying meridional transport, either over the Arabian Sea interior or the western boundary current/Somali Current, can, with considerable confidence, be estimated by the monthly-varying wind stress curl via the time-independent Sverdrup relation applied in a straightforward way.[20]

To be sure, the scatter diagram of Fig. (16), lower, gives pause to this last claim, as some monthly

[20]Something to note: the monthly winds are (auto-)correlated in time and especially within a season. A similarly high correlation would not hold if the monthly wind varied randomly.

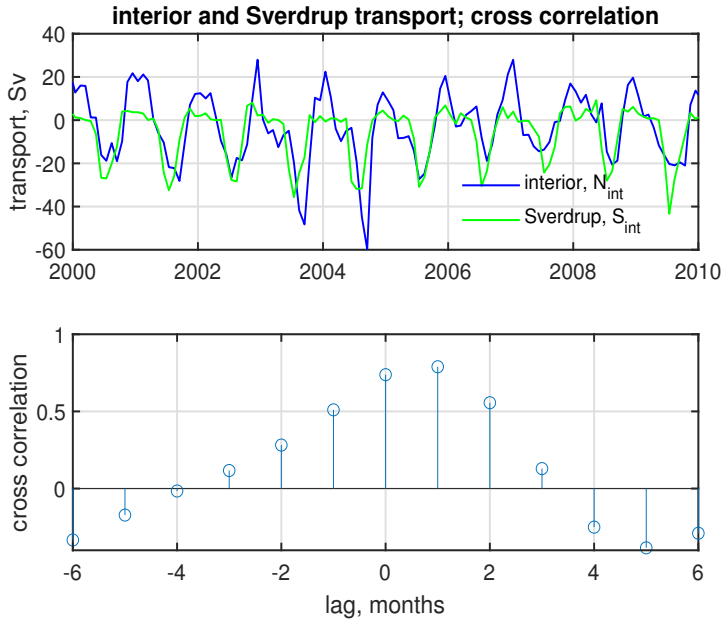

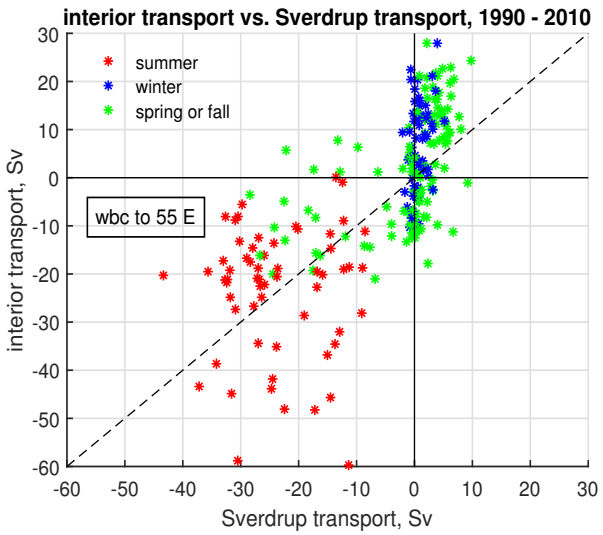

Figure 16: **(top)** Meridional volume transports across the 10 N interior boundary as computed from SODA meridional velocity, $N(t)_{int}$, (blue line) and as estimated from stress curl and the Sverdrup relation, S_{int}, (green line). **(middle)** Lagged cross-correlation between $N(t)_{int}$ and $S(t)_{int}$. The small asymmetry indicates that N_{int} lags S_{int} by about two to three weeks. **(lower)** Scattergram of monthly N_{int} and S_{int} with season color-coded. The S_{int} gives some account of the year-to-year variation in the amplitude of the summertime, Southwest Monsoon season transport (red markers), though with considerable scatter about the 1-to-1 line. The same can not be said of the wintertime, Northeast Monsoon transport (blue markers) when the actual transport systematically exceeds the Sverdrup transport. Notice the very large asymmetry in the distribution of data overall, a reflection of the summer to winter difference in volume transport magnitude.

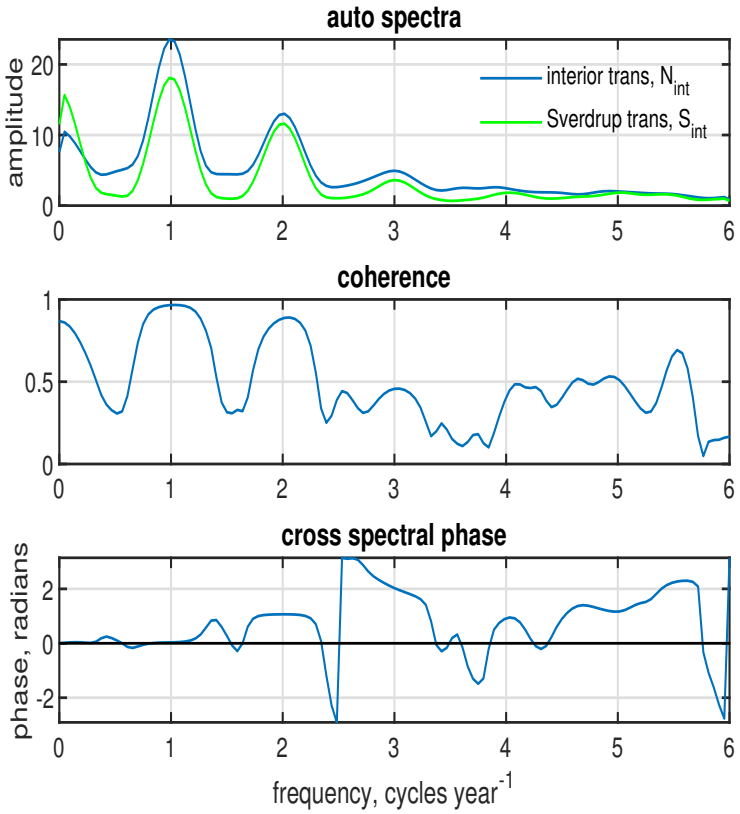

Figure 17: Frequency domain analysis of meridional transport across the 10 N interior from SODA reanalysis and Sverdrup transport for the two decade period 1990 - 2010. **(top)** Auto spectrum of $N(t)_{int}$ and $S(t)_{int}$ showing significant peaks at 1 cycle per year, and a secondary peak at 2 cycles year^{-1}. These peaks are broadened considerably by averaging over six frequency bands which is required to estimate coherence; these peaks are quite narrow when estimated via a periodogram. **(middle)** Coherence between $N(t)_{int}$ and $S(t)_{int}$, which is high at the annual and semi-annual frequencies. **(lower)** Phase; at the annual frequency, the phase is not distinguishable from zero.

estimates are far from the one-to-one line. Some of this is due to eddy variability, which is quite strong anywhere near the western boundary, e.g., the Great Whirl and especially the Socotra Eddy, which is usually near 10 N but is not stationary in space or time. The eddy contribution to this transport estimate might presumably be suppressed somewhat by choosing a wider western boundary region, say the Somali coast to 58 E, and thus including almost the entire Socotra Eddy within the western boundary segment, and leaving less of it within the interior. With that change, the maximum lagged correlation goes up to 0.9, and the scatter diagram for summer tightens up considerably (Fig. 18). There is no significant change for the winter estimates. The first definition for the western boundary region made here, 55 E, the Findlater Jet axis, was plausible *a priori*, and so will be retained pending a better means for discriminating the Somali Current from eddy variability.[19]

The auto spectra and the coherence reveal a second significant peak at 2 cycles per year, the semi-annual frequency. This is not immediately apparent to the eye in the monthly time series, but after a second or third look you may notice some higher frequency (than annual) variability that is most apparent in winter, when the transport is smaller. A semi-annual variation of wind stress is quite prominent along the equator, where the sun goes directly overhead twice a year (March on the way north, September on the way south), and evidently this semi-annual variability reaches to at least 10 N (in the SODA reanalysis). The coherence is high also at this semi-annual frequency, and the phase lag is about 0.5 radians, with the sign indicating that the semi-annual meridional transport lags the semi-annual Sverdrup transport by several weeks to a month.

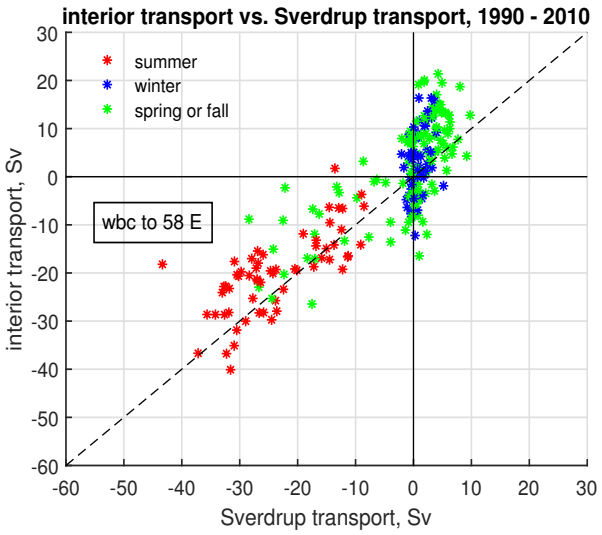

Figure 18: Scattergram of monthly N_{int} and S_{int} with season color-coded. This is exactly Fig. (16) with the exception that the eastern edge of the western boundary region was extended three degrees east to 58 E.

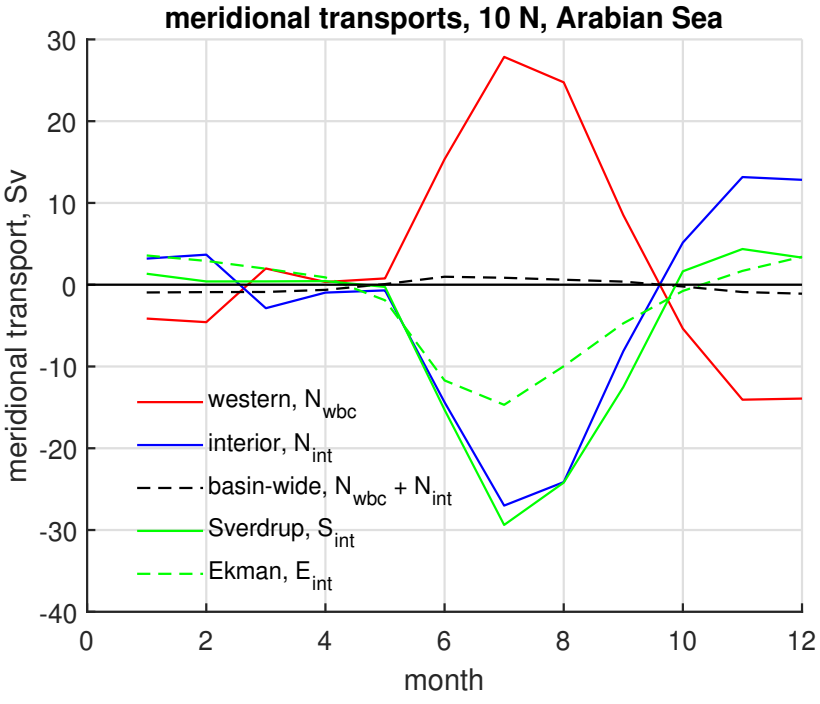

Figure 19: A composite average annual cycle of meridional volume transports across 10 N in the Arabian Sea computed over 2002 through 2006. Transport is evaluated over a western boundary region, N_{wbc} (solid red line), and over the interior, all the rest of the basin to the east, N_{int} (solid blue line). The dashed black line is their sum, $N_{wbc} + N_{int}$, which should be very small compared to either the wbc or interior transports as in the previous figure. The green line is the composite average Sverdrup transport by month, S_{int}, estimated from wind stress curl along the interior segment of the 10 N boundary. The Sverdrup transport has very similar magnitude and phase to the interior transport during the summer months of the Southwest Monsoon, but not so during the winter, when it is considerably less than the interior transport.

5.4 Summary of the description

The wind-driven circulation of the Arabian Sea has been framed in very specific (and one could say narrow) terms, *viz.,— where, when* and *why* is there meridional transport across 10 N?

Where. Meridional transport is strongest within a western boundary region several hundred kilometers wide (Figs. 6 and 19) that includes the summertime Somali Current. A closely compensating meridional transport occurs over the interior of the basin. The summertime circulation of the Arabian Sea is thus not unlike the time-mean circulation of the North Atlantic subtropical gyre. One difference in detail is that the interior transport is considerably stronger toward the western side of the basin, as is the wind stress curl. This appears to be a significant aspect of the time-dependent response discussed further in the next section, Swec. 10.6.2.

When. The meridional transport (and the flow generally) shows a very striking seasonal variation. The western boundary region includes a northward Somali Current in summer, having a magnitude of roughly 20 - 40 Sv. On average over several decades the maximum summertime transport is about 30 Sv. This northward flow is usually established within a few weeks of the onset of the Southwest Monsoon winds at 10 N. There is a considerably weaker and less well organized southward flow in the western boundary region during the winter, about 10 Sv.

Why. The results to here demonstrate that the Sverdrup relation plus wind stress curl give a fairly good account of the seasonal, and even the monthly, meridional transport across interior and western boundary regions of 10 N in the Arabian Sea. This is at least slightly surprising, and before concluding that the Sverdrup relation explains the meridional transport, it is necessary to explain why the Sverdrup relation is relevant, i.e., why the Sverdrup relation should make a plausible estimate of the summertime meridional transport.[21]

The Sverdrup relation predicts amplitude. So far as time goes, the Sverdrup relation taken literally indicates that the meridional transport should track the stress curl instantaneously. Clearly this can not be true, which is perhaps the reason that the Sverdrup relation has been somewhat overlooked in this context. However, the Arabian Sea circulation responds quickly enough — within a few weeks — that the Sverdrup relation makes a fairly good approximation of the link between the seasonally-varying (and even the monthly-varying) winds and circulation. As noted in the introduction, the same response time for a mid-latitude basin is roughly 1500 days (Sec. 5.4, Part 4), or two orders of magnitude greater. This suggests a slightly sharper question: why this very large difference between the Arabian Sea and the subtropical North Atlantic?

The experiments and results of Sec. 6, Part 4 show that an important parameter in the adjustment of

[21] Suppose that the issues surrounding time-dependence can be put aside. Would the Sverdrup relation then make a good explanation of the transport? Another example: suppose that a current is known to be geostrophic balance. Would geostrophy make a good explanation of the currents? I would say no, not if that is all that is on offer. To make a good explanation requires an explanation of why geostrophy should hold in the case at hand (to be sure, these circumstances are so common that geostrophy is often taken for granted), and better, explain how the pressure field came to be established. Here the task is to explain why Sverdrup should hold, given the significant time-dependence of the phenomenon.

a typical midlatitude basin to steady, baroclinic Sverdrup flow will in many cases be the east-to-west basin transit time for a first mode baroclinic, long Rossby wave having a phase and group speed $C_{Ro} = \beta R_d^2$. Applied to the Arabian Sea ($L_{basin} = 2500$ km) this gives an estimate

$$T_{basin} \; = \; \frac{L_{basin}}{\beta {R_d}^2} \; = \; L_{basin} \frac{f^2}{\beta C^2} \; \approx \; 100 \;\; \text{days.} \tag{5}$$

This basin transit time is appropriate when the wind stress field is independent of x, and the basin width, L_{basin}, is the relevant, zonal, external length scale. The ratio of this T_{basin} evaluated at 10 N Arabian Sea vs T_{basin} at 30 N in the subtropical North Atlantic is about 0.05, or a factor of about 20. Thus, latitudinal dependence and the reduced basin width of the Arabian Sea go a long way towards explaining the very large difference in response times. However, such a large extrapolation is not entiely convincing, and in any event (5) comes up short of the factor O(10^2) that characterizes the ratio of Arabian Sea and subtropical gyre response times.

6 Experiments with western-biased, jet-like winds show a very fast adjustment

It is helpful to consider briefly two additional numerical experiments that are configured as a highly idealized Arabian Sea basin driven by a jet-like wind field. These experiments will reveal another factor of roughly 5 that favors a fast response of the Arabian Sea. The basin is taken to be rectangular, 4000 km north-south extent, centered on the equator, and 2500 km east-west. A three-layer stratification, including a free sea surface, is as before, though with a slightly thinner (shallower) thermocline that gives a slightly reduced baroclinic fist mode gravity wave speed, C = 2.6 m sec^{-1} and a baroclinic radius of deformation $R_d \approx 100$ at 10 N latitude.

An important difference vis-a-vis a typical mid-latitude basin arises from the Southwest Monsoon wind stress field. As noted in Sec. 3.1, the summertime Arabian Sea wind stress is mainly the Findlater Jet, which is as much meridional as it is zonal, and is present over the western side of the basin (Sec. 3). To model this, the wind stress field will be taken as meridional only, and given a jet-like, hyperbolic secant profile that is independent of y,

$$\tau_y(x,t) = \tau_o(t) sech((x - x_o)/L_{jet}), \tag{6}$$

the red line of Fig. (20), right. The jet axis is set on x_o = -850 km, which is 400 km from the western boundary, and the jet width $L_{jet} = 300$ km. The issue here is time-dependence, not amplitude, and so in this first experiment the wind stress amplitude is taken to be a nominal $\tau_o = 0.1$ Pa. In order to minimize inertial motions and short Rossby waves, the wind stress amplitude was ramped up from zero to τ_o in the first 20 days of the experiment and thereafter held constant. The most important result from these experiments will be apparent in this small amplitude (linear) case. However, finite amplitude (nonlinear) effects are in some respects very interesting and will be investigated in a second experiment (Sec. 7) having a more realistic wind stress amplitude, $\tau_o = 0.5$ Pa.

A plan view of the solution at 30 days after startup and time series of the transport in each layer are in Figs. (20) and (21). The dominant feature of the circulation is an anticyclonic gyre that is mainly in the western half of the basin. This gyre is elongated north to south compared with the real Arabian Sea gyre, no doubt because the model wind jet does not turn clockwise over the basin, as does the real, terrain-following Findlater Jet (Fig. 3). It is notable that the volume transport almost keeps pace with the wind stress (cf. the black and cyan lines of Fig. 21) lagging by less than a week on average. In Sec. 8, Part 4 it was noted that a barotropic, quasi-steady Sverdrup response sets up very quickly, within a week or two even within a large, mid-latitude basin. In that light, the (almost) quasi-steady barotropic response of a relatively small, low latitude basin is not at all surprising — it should happen, and is part of the reason why the Sverdrup relation gives fairly good estimates of the monthly transport in the Arabian Sea.

6.1 Baroclinic Sverdrup flow

However, a fast barotropic response can not be the whole story; the Somali Current would hardly be noticed if it was strictly barotropic. Rather, the Somali current is significantly surface-intensified, i.e., it is baroclinic and equivalent barotropic, Fig. (8), right, and see, e.g., Düing and Szekielda (1970)[1], which the Sverdrup relation by itself does not explain. The experiments of the previous sections provide some additional guidance.

Sverdrup transport is the sum of geostrophic and Ekman transports (Sec. 3.1, Part 4),

$$S_{int} \;=\; G_{int} \;+\; E_{int}\,,$$

where the

$$E(t)_{int} \;=\; \frac{1}{\rho f}\int_{India}^{55E} \tau_x(x,y_o,t)\;dx$$

can be readily evaluated. During the summertime Southwest Monsoon, the Ekman transport is estimated to be about a third or even up to a half of the Sverdrup transport, Fig. (19). Ekman transport sets up very quickly, essentially in phase with the wind stress, and is strongly surface-intensified, being confined to the shallowest 50 - 100 m, at most. Hence, the Ekman transport can account for a significant part of the surface-intensified Sverdrup flow in the interior. Of course, this applies to the SODA reanalysis (and the real Arabian Sea) where there is a zonal component of the wind stress, but not to the new model solution where the winds are meridional only and hence there is no meridional Ekman transport.

Within the western boundary region of the model solution, the upper layer transport (upper 250 m) lags the stress curl by only about one to two weeks (estimated by inspection of the red and magenta lines of Fig. 21), and after only about three weeks, most of the Sverdrup transport is found within the surface layer. This is considerably faster than would be expected from the usual, baroclinic basin transit time, Eqn. (5). The wind field over the Arabian Sea, and specifically the Findlater Jet, is likely to be an important factor insofar as the most important zonal length scale in this experiment comes from the wind field, L_{jet}, as in the experiments of Sec. 7.3, Part 4, rather than the basin width, as assumed in Eqn. (5) and which is appropriate when the wind is purely zonal and varies only in the meridional direction. The

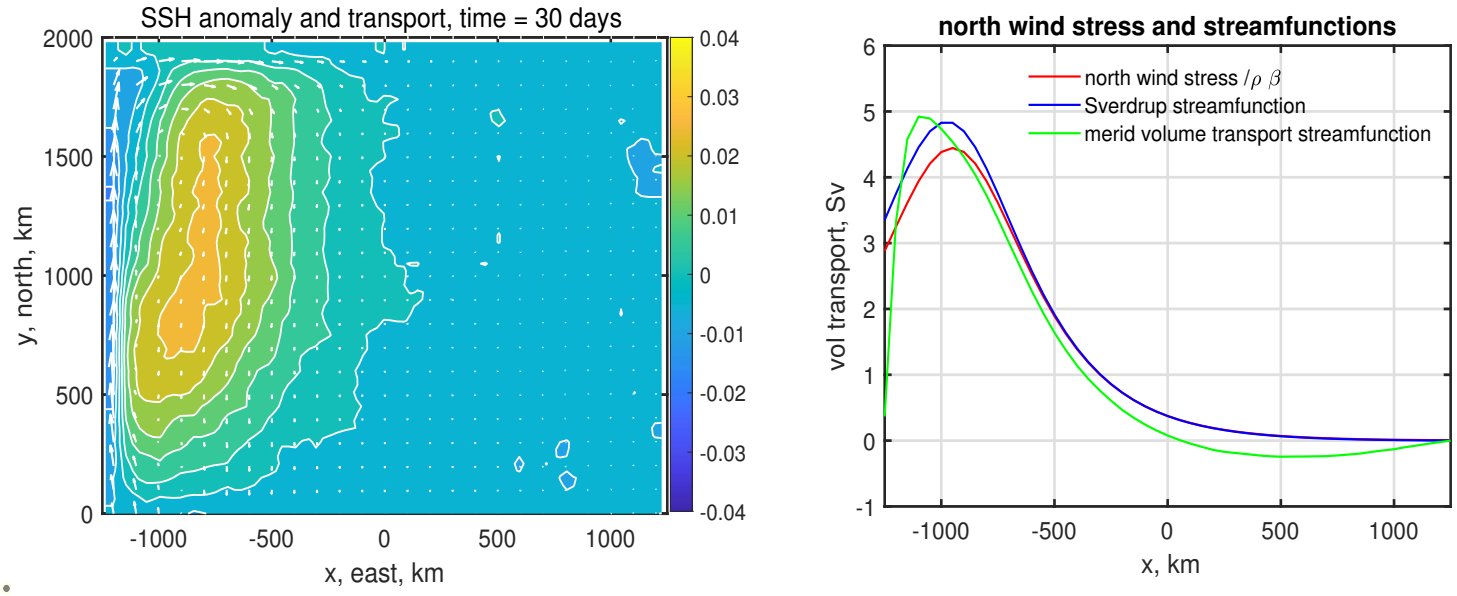

Figure 20: **(left)** A plan view of the northern half of the Arabian Sea model domain at 30 days after the start of the small amplitude experiment ($\tau_o = 0.1$ Pa). The background color depicts the ssh anomaly (scale at right is in meters), and the vectors are volume transport. The pattern of ssh includes a maximum that is almost coincident with the wind stress jet axis, and the transport occurs in a nearly geostrophic flow that is more or less along the flanks of the ridge, though compressed somewhat onto the western boundary. **(right)** Wind stress and volume transport streamfunctions for the small amplitude experiment (note the small values of transport). The wind stress zonal profile is the red line (scaled here with $\rho\beta$) and the corresponding Sverdrup streamfunction is blue. The meridional transport streamfunction $\Psi(x)$ sampled 30 days after the start is in green. A question for you: Can you explain why the scaled wind stress and the Sverdrup streamfunction are (almost) identical?

response time estimated with $L_{jet} = 300$ km is, from Eqn. (5),

$$T_{jet} = \frac{L_{jet}}{\beta R_d^2} \approx 15 \text{ days}, \tag{7}$$

and which is O(10^{-2}) compared to the basin transit time of the North Atlantic subtropical basin. One way to think of this is to note that the entire Arabian Sea basin does not contribute equally to the Sverdrup transport (as it will in a basin driven by the shear between the eastward and westward global wind belts) simply because the wind stress curl is by far strongest within a few hundreds of kilometers of the western boundary.[22]

[22]There is another way to think about this adjustment to steady Sverdrup flow that you may find more physical. First, compute(estimate) the wind-forced Ekman pumping, and then the corresponding geostrophic current, which will be meridional and time-dependent. This has previously been dubbed the Stage 2, locally-forced current. Suppose that a steady state will be achieved when the beta effect acting upon this current is just sufficient to cancel the Ekman pumping. Ignoring spatial phase(!) and assuming a hard start-up of the wind stress, the time this takes is just (7). If L_{jet} is the relevant horizontal scale, and if geostrophy and beta are of leading importance, then (7) seems inevitable.

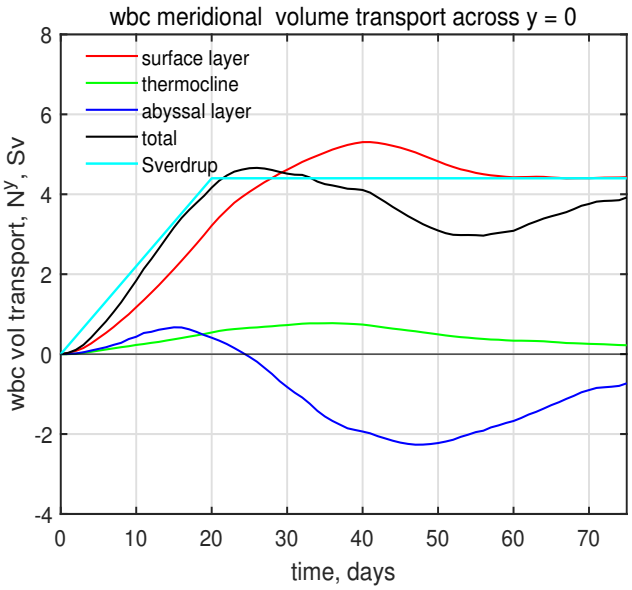

Figure 21: Time series of the meridional transport within the western boundary region at the equivalent of 10 N and in the small amplitude experiment. The Sverdrup transport, which is proportional to the time-dependent wind stress divided by $\rho\beta$, is the cyan line, and the volume transport over the full water column is the black line. Notice that the volume transport almost keeps pace with the Sverdrup transport. The volume transport within each of the three model layers are the colored lines. The surface layer transport (red line) lags the Sverdrup transport by only about one to two weeks.

6.2 Summary, why the Sverdrup relation is relevent

This simple experiment indicates that a baroclinically adjusted, surface-intensified Sverdrup flow may be expected within the western Arabian Sea within only a few weeks of the onset of (Findlater) jet-like Southwest Monsoon winds. This very fast response (compared to a mid-latitude ocean basin) is due mainly to the low latitude of the basin, Eqn. (5), and enhanced significantly by the western-biased and jet-like structure of the Southwest Monsoon wind field. These lead to an estimate of the baroclinic response time, Eqn. (7), of about two weeks, which is consistent with the idealized model solution, Fig. (21),and the SODA reanalysis soliution.

7 Appendix: Finite amplitude effects — is that a great whirl?

The nearly linear solution described above misses an interesting finite amplitude effect that arises in a second experiment in which the wind stress amplitude is set to a more realistic value, $\tau_o = 0.5$ Pa. The meridional velocity within the surface layer of the western boundary current then becomes very large within a few tens of days, exceeding 2 m sec^{-1}, which is not inconsistent with the largest observed speeds observed within the summertime, Somali Current (Düing and Szekielda, 1970[1]).

7.1 Froude, Ekman and Rossby numbers

A rough idea of the likelihood of finite amplitude effects can be gleaned from estimates of several nondimensional numbers that may be formed given values of the current, $U = 2$ m sec^{-1}, the Coriolis

parameter (at 10 N) $f = 2.5 \times 10^{-f}$ sec^{-1}, $\beta = 2.3 \times 10^{-11}$ sec^{-1} m^{-1}, the wind stress, $\tau_o = 0.5$ Pa, the gravity wave phase speed, $C = 2.6$ m sec^{-1}, an along stream length scale, $L = 1000$ km (by inspection of Fig. (20), left), and an eddy length scale, $L_{eddy} = 200$ km (same comment). These may be combined into more or less familiar ratios,

- wind stress Ekman number, $\frac{U^2}{L} / \frac{\tau_o}{\rho_0 h1} \approx 0.8$,
- Froude number, $U/C \approx 0.7$,
- eddy Rossby number, $\frac{U^2/L_{eddy}}{fU} = U/fL_{eddy} \approx 1.2$.

From the first of these it is evident that the inertia of the current $\propto U^2/L$ is appreciable compared to the wind stress (the Ekman number is O(1)) and to the possible baroclinic pressure gradient (the Froude number is also O(1)).[23] As a consequence of the large currents, there are substantial finite amplitude (nonlinear) effects, by horizontal advection and by large changes in layer thickness.[24]

Despite the large currents and thickness gradients of this second experiment, there is more in common with the the small amplitude solutions than might have been expected, cf. Figs (20) and (21) with Figs. (22) and (23). The amplitude of the circulation in the new experiment is about 5 times that of the former, consistent with the ratio of the wind stresses and so the circulation amplitude is quasi-linear in τ_o. The rise time (response time) of particular interest here also appears to be about the same as in the small amplitude experiment, and so the response time is also is a linear phenomenon (i.e., is independent of τ_o). Notice, though, that there are quite large oscillations in the transport, and most notably an initial, positive overshoot by about 50%.

The most obvious difference made by finite amplitude effects is the appearance of a comparatively small, roughly 300 km diameter, anti-cyclonic eddy that on day 30 is at about $(x,\ y) = (-1000,\ 700)$ km. This eddy is adjacent to the western boundary current, not the basin boundary, and it is somewhat to the south of and almost separated from the main gyre. This eddy begins to form at about day 15, and then strengthens as it moves very slowly toward the north. By day 30 it has an azimuthal transport of about 15 Sv, which is comparable to the western boundary current. Depending upon just where this eddy sits with respect to the presumed eastern edge of the western boundary region, it can thus have a substantial impact

[23] An excellent article discussing the many forms and interpretations of a Froude number is available online at https://en.wikipedia.org/wiki/Froude_number

[24] Large indeed: in the northwestern corner of the model domain the surface layer thickness goes to almost zero at about 60 days after the start of the experiment, and of course that immediately sets off a figurative 'KaBoom' in the numerical integration. This is a shortcoming of the present numerical model and its layered representation of the momentum and continuity equations. The cure is twofold. First, utilization of a gridded finite difference representation in the vertical so that division by a material layer thickness is not needed. Second, a representation of upper ocean vertical mixing which will help keep the Ekman layer at a reasonable thickness even in the presence of very large and sustained wind stress and upwelling. Both of these are an integral part of the Regional Ocean Modeling System (ROMS), which is thus much better suited to a detailed simulation of the Somali Current than is the present, elementary layered model. For more on ROMS, see https://en.wikipedia.org/wiki/Regional_Ocean_Modeling_System (you may have to type this into your browser).

upon the estimated western boundary current transport, and just the complementary effect on the interior meridional transport, Sec. 5.2.

7.2 Speculation on an eddy formation process

An eddy formation process might be characterized in any of several ways, e.g., by a momentum, vorticity or energy balance, but here the discussion emphasizes phenomenology, i.e., what can be seen in this solution and in the SODA solution (Fig. 1). Hurlbert and Thompson (1980)[1] emphasized that the Somali Current is an inertial western boundary current in the sense that it has the potential to overshoot the region where it is generated by and be in approximate balance with a wind stress and stress curl. The best-known example of such an inertial boundary current is provided by the the western boundary current of a multi-gyre circulation of the sort considered in Sec. 5.5, Part 4. The northward-going subtropical western boundary current will have enough inertia to cross the wind stress curl-defined gyre boundary and intrude a significant distance into the adjacent subpolar gyre where it will be far out of balance with the prevailing wind stress curl. Potential vorticity conservation will tend to bring the intruding current back into its home gyre, likely triggering a Rossby wave, and/or, the intruding current may form a cutoff ring or eddy. It is speculated that something similar could occur in space and time in the Arabian Sea. The qualitative evidence for this in the SODA solution is that during early summer, the western boundary current (Somali Current) forms first at lower latitudes, where the Southwest Monsoon onset occurs first, and extends for few hundreds of kilometers northward along the coast. The current then detaches from the western boundary and rolls up into a fairly large (300 km diameter), anticyclonic eddy. This typically happens several times during early summer, eventually forming something like a Great Whirl in the reanalysis solution. In the present experiment, in which the wind field is fixed in space but time-dependent, the adjustment to Sverdrup flow occurs first at lowest latitude, and progresses northward as discussed in Sec. 7.3, Part 4. From Eqn. (87), the y-dependent rate of the northward progression evaluated at $y_o = 1000$ km is

$$V_{Sv} = \frac{C^2}{2\beta L_\tau y_o} = 0.7 \text{ m sec}^{-1}.$$

This is comparable to but a little less than the northward current speed within the western boundary current (which is, of course time-dependent). Thus the northward flowing western boundary current could outrun the adjustment to Sverdrup flow. A variant on this is that a sufficiently fast western boundary current may also outrun the northward translation of the ITCZ, $V_{itcz} \approx 0.4$ m sec^{-1} (Sec. 3.2), and thus the Southwest Monsoon onset (this is not relevant in the present numerical experiment in which the wind is switched on over the entire model domain at once). These ratios of northward speeds may be written as Froude numbers,

- Sverdrup adjustment Froude number, $F_{Sv} = U/V_{Sv} \approx 3$,
- ITCZ translation Froude number, $F_{itcz} = U/V_{itcz} \approx 5$,

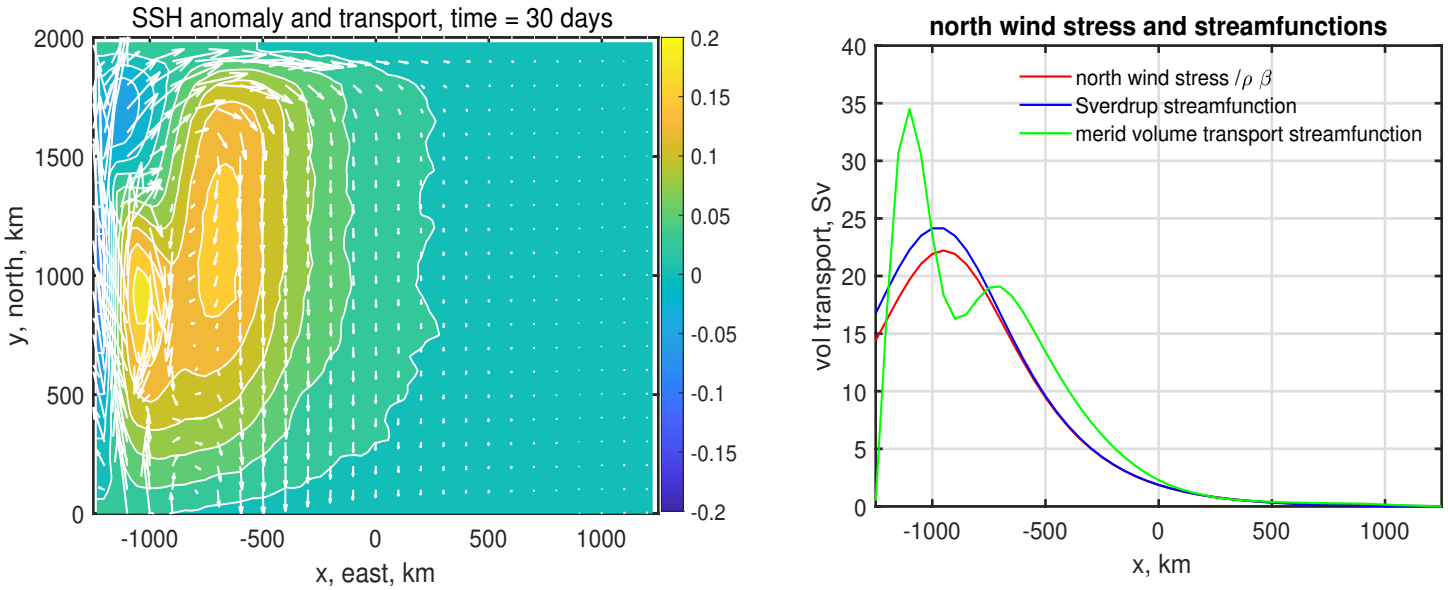

Figure 22: **(left)** A plan view of the Arabian Sea model domain, 30 days after the start of the large amplitude experiment ($\tau_o = 0.5$ Pa). The background color depicts the ssh anomaly (scale at right is in meters), and the vectors are volume transport. Compare this with the small amplitude (linear) solution of the two previous figures. **(right)** Wind stress and volume transport streamfunctions. The wind stress zonal profile is the red line (scaled here with $\rho\beta$) and the corresponding Sverdrup streamfunction is blue. The meridional transport streamfunction $\Psi(x)$ sampled 30 days after the start is in green. Note that the amplitude here is about five times that of the small amplitude experiment, Fig. (21), right, and that there is a large mismatch between Sverdrup and actual meridional transport near the western boundary.

though they do not scale the magnitude of terms in a momentum balance in the way that the conventional Froude number does.

It is fair to say that this eddy is the great whirl (n.b., l/c) of the present model, but could it be an analogue of the real Great Whirl of the Arabian Sea? It has several properties in common with the Great Whirl — approximate size, amplitude comparable to the central gyre, location compared to central gyre, and movement. However, the genesis process is not in common. Beal et al. (2013)[14] and references therein, as well as the data displayed in the animation of Fig. (1), make a compelling case that the real Great Whirl begins in the spring when the 6 N ridge intersects the western boundary, a process not included in this simulation. In most years this occurs weeks before the Southwest Monsoon onset. Thereafter the Great Whirl strengthens alongside the wind-driven Somali Current, which could be in common with the present eddy formation.

8 Concluding remarks

The plan for this essay was to provide a concise description of the seasonally-varying circulation of the Arabian Sea (summarized in Sec. 5.4 and not repeated here), and the specific goal was to construct an explanation of the link between the winds and the circulation that would entail the observed, rapid

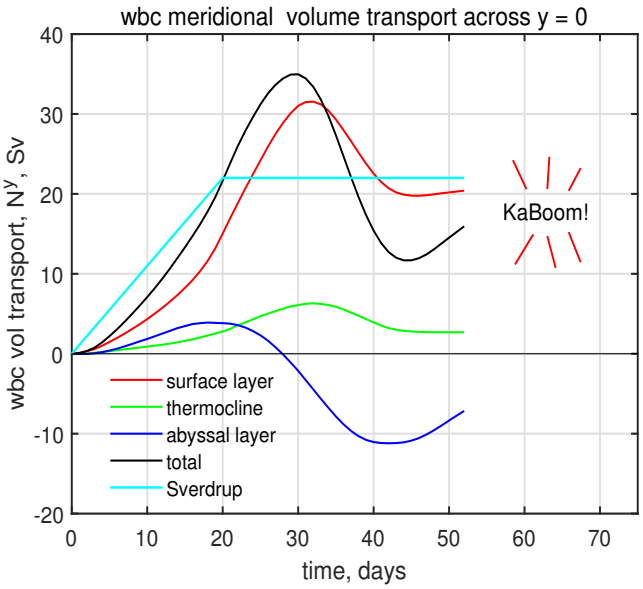

Figure 23: Time series of the meridional transport within the western boundary region of the large amplitude experiment, cf. the small amplitude experiment of Fig. (20). An untoward event at about 60 days is discussed in the main text and footnote 24.

response to the monsoon winds. The intent was that the explanation should be as simple as possible, but not simpler.[25]

It is very seldom that we will have the opportunity to adjudicate simplicity among a collection of otherwise suitable explanations, but we do have the freedom to choose a new problem and to define a question that might lead to a useful, simple explanation. The key in this case was a narrow focus on the meridional transport into and out of an Arabian Sea control volume that was open along one latitude, 10 N. And then, the time-dependent transport across 10 N was represented by just two components, an interior piece, $N(t)_{int}$, and the complementary western boundary piece, $N(t)_{wbc}$. Since

$$N(t)_{wbc} \approx -N(t)_{int}, \tag{8}$$

this reduced the spatially complex circulation of the Arabian Sea to one variable, the meridional transport integrated over the interior of the basin, a span of about 2000 kilometers. It was found that

$$N(t)_{int} \approx S(t)_{int}, \tag{9}$$

with S the Sverdrup transport evaluated on monthly wind stress curl (Sec. 5.3). It was argued that the Sverdrup relation may be regarded as an explanation of the link between the wind and the Arabian Sea

[25] This famous aphorism has been distilled from rather more emphatic advice offered by Albert Einstein, "It can scarcely be denied that the supreme goal of all theory is to make the irreducible basic elements as simple and as few as possible without having to surrender the adequate representation of a single datum of experience." A. Einstein, On the Method of Theoretical Physics, The Herbert Spencer Lecture, Oxford, England, June 10, 1933. Einstein was a keen student of physics generally, including fluid mechanics, and wrote his PhD thesis on the variation of viscosity with the molecular size of a solute. His aim was to support the then tenuous molecular hypothesis. Einstein later developed an insightful theory on erosion and sediment deposition in meandering river flows by analogy with the centripetal motion of tea leaves suspended in the bottom boundary layer of a swirling cup of tea, https://www.ias.ac.in/article/fulltext/reso/005/03/0105-0108 (you may have to type this into your browser). No one of Einstein's generation could have been a witness to the eddy variability and complexity of the ocean circulation in the way that we are today thanks to satellite observations. Here's an entirely hypothetical question for you: If Einstein had seen the animation of Arabian Sea circulation, Fig. (1), would he have insisted that a theory of the Arabian Sea must represent every single datum of that experience?

circulation because of the very fast response of baroclinic Sverdrup flow, which follows from the low latitude of the Arabian Sea and the jet-like form of the Southwest Monsoon wind field (Sec. 6.2).

There is no doubt that Eqn.(9) is simple, but does it explain enough? A two component representation of the circulation Eqn. (8) is a very low resolution view of a spatially and temporally complex flow field, and it is fair to ask: Has the Arabian Sea circulation been made too simple? The opening remarks suggested one possible criterion for judging the utility of the annual mean circulation, *viz.*, does it represent an observable state of the circulation? The answer in the case of the Arabian Sea is a fairly clear 'no', which motivated a look at the seasonal circulation. So now let's suppose that the seasonal mean is known — but does that look like an observable state of the circulation? The data in Fig. (10) allow an informal test, and a generous assessment might be 'just barely', but you can decide for yourself.

What is clear is that there is much more to learn about the Arabian Sea circulation than is contained within this brief and limited introduction. The best result is that it might spark your curiosity and a desire to make your own contribution.

9 Problems

(1) Using the animation of the data of Fig. (1), consider the following. The ITCZ is not sketched onto the frames, and it isn't readily apparent as a shear line or divergence maximum in the stress field. However, the associated wind reversals, especially the onset of the Southwest Monsoon, are clearly evident. Pick a latitude along the western boundary: How long after the passage of the sun does the wind reversal occur? Does this vary with latitude? Is there anything special about the near-equatorial region? Is there any obvious temporal variation in the wind field aside from the marked seasonal variation?

(2) During the discussion of the streamfunctions of Fig. (7), it was noted that the streamfunction should go back to near zero on the western boundary, presuming only that the net volume transport through the 10 N section is small compared to the regional volume transport. We also noted that the ssh (geostrophic) slope has the sign of the meridional transport, and is generally large where the transport is large. However, the ssh does not return to its starting value going from east to west across the basin; the interior slope is smaller by a factor of two or three than is needed to accomplish this. Any thoughts on why that might be the case? A second question: How are the annual mean and the seasonal mean streamfunctions related?

(3) Using the animation linked in Fig. (1): When are the first signs of the Great Whirl? When does it reach a maximum amplitude? How quickly does the Great Whirl expire after the wind reversal in the fall? How about the Socotra Eddy? Can you discern a relationship between these eddies (don't forget SEII) and the somewhat larger anti-cyclonic gyre identified with the interior Sverdrup flow? Which develops first, the gyre or the eddies?

(4) Questions regarding remote forcing seen in the animation https://www2.whoi.edu/staff/jprice/NIO-ssh/. Do you see any evidence that the western basin of the NIO (the Arabian Sea) can have a significant impact upon the eastern basin (the Bay of Bengal), or is remote

forcing one way only, i.e., westward only? Is there evidence of remote forcing from the equator?

(5) How does the western boundary region mismatch of meridional transport and Sverdrup transport seen in Fig. (13) show up in the Sverdrup streamfunction? What sets the western boundary value of the Sverdrup streamfunction?

(6) The net transport through 10 N (the black line of Fig. 15) has an amplitude of roughly 1 Sv, and oscillates with an annual period. Could this possibly be a genuine signal of ssh variation over the control volume (as opposed to a sampling issue with the velocity)? The surface area of the control volume is about 2.5×10^6 km^2.

Index

Resource: Topics in Fluid Dynamics

James Price